Data Mining and Knowledge Discovery (2023) 37:2139–2191
https://doi.org/10.1007/s10618-023-00940-w

Interplay between topology and edge weights in real-world graphs: concepts, patterns, and an algorithm

Fanchen Bu[1] · **Shinhwan Kang**[2] · **Kijung Shin**[1,2]

Received: 24 November 2022 / Accepted: 5 May 2023 / Published online: 26 July 2023

Abstract

What are the relations between the edge weights and the topology in real-world graphs? Given only the topology of a graph, how can we assign realistic weights to its edges based on the relations? Several trials have been done for *edge-weight prediction* where some unknown edge weights are predicted with most edge weights known. There are also existing works on generating both topology and edge weights of weighted graphs. Differently, we are interested in generating edge weights that are realistic in a macroscopic scope, merely from the topology, which is unexplored and challenging. To this end, we explore and exploit the patterns involving edge weights and topology in real-world graphs. Specifically, we divide each graph into *layers* where each layer consists of the edges with weights at least a threshold. We observe consistent and surprising patterns appearing in multiple layers: the similarity between being adjacent and having high weights, and the nearly-linear growth of the fraction of edges having high weights with the number of common neighbors. We also observe a power-law pattern that connects the layers. Based on the observations, we propose PEAR, an algorithm assigning realistic edge weights to a given topology. The algorithm relies on only *two* parameters, preserves *all* the observed patterns, and produces more realistic weights than the baseline methods with more parameters.

Keywords Data mining · Graph mining · Weighted graph analysis · Real-world graph analysis · Edge-weight estimation

Responsible editor: Charalampos Tsourakakis.

✉ Kijung Shin
kijungs@kaist.ac.kr

Fanchen Bu
boqvezen97@kaist.ac.kr

Shinhwan Kang
shinhwan.kang@kaist.ac.kr

[1] School of EE, KAIST, Daejeon, South Korea

[2] Kim Jaechul Graduate School of AI, KAIST, Seoul, South Korea

1 Introduction

In weighted graphs, the edge weights reveal the heterogeneity of edges and enrich the information provided by the topology (Newman 2004). In practice, weighted graphs have been widely used to model traffic (De Montis et al. 2007), biological interactions (Aittokallio and Schwikowski 2006), personal preference (Liu et al. 2009), etc. The relation between topology and edge weights, therefore, attracts much attention. A typical scenario where the two kinds of information are integrated is *edge-weight prediction* (Fu et al. 2018; Rotabi et al. 2017). The target of edge-weight prediction is to predict the unknown edge weights using the given topological and edge-weight information, where usually most of the edge weights are given as the inputs. Another related direction is to generate both the topology and the edge weights of weighted graphs (Akoglu et al. 2008; McGlohon et al. 2008; Yang et al. 2021).

However, not much has been explored about the relation between the pure topology and the edge weights in a graph, despite the importance of the relation. In some previous trials, the problem of classifying edges into strong ones and weak ones by assuming strong triadic closure (Sintos and Tsaparas 2014) (STC) is considered. The STC assumption forbids open triangles (also called triads or wedges) with two strong edges and aims to maximize the number of strong edges. However, the diversity of edge weights is over-simplified in such a setting. Moreover, it has been pointed out by Adriaens et al. (2020) that the STC assumption with a maximum number of strong edges is often far from the reality, and the generalized version still has room for improvement, especially w.r.t the empirical grounds (Adriaens et al. 2020).

Specifically, we study how the edge weights in real-world graphs are related to the topology *in a macroscopic way*, which allows us to generate realistic edge weights when given an unweighted topology. We would like to emphasize that we do not aim to assign edge weights with small errors w.r.t each individual edge. We are motivated by the following practical applications:

- *Edge weight anonymization.* In social networks, due to data privacy issues, sometimes only the binary connections are publicly accessible, while the detailed edge weights should not be publicized (Steinhaeuser and Chawla 2008; Skarkala et al. 2012). Using the macroscopic patterns, we are able to generate realistic edge weights for a given topology and publicize the generated weighted graph to researchers and practitioners as a benchmark dataset, without revealing the true edge weights.
- *Anomaly detection.* In communication networks, the edge weights usually represent the frequency or intensity of the communication between the entities. Using the patterns observed on real-world graphs, we may detect anomalous edge weights that deviate from the patterns, and they may correspond to entities that have abnormally frequent or intensive communication (Thottan et al. 2010; Akoglu et al. 2015).

- *Community detection.* Community detection is a fundamental problem in network analysis (Fortunato 2010). Edge weights are known to be helpful for community detection because they provide additional information about the strength and importance of connections between nodes (Liu et al. 2014; He et al. 2021), and thus assigning edge weights to unweighted graphs has the potential to enhance the performance of community detection algorithms (Berry et al. 2011).[1]

We introduce and use a new tool called *layers* to study weighted graphs in a hierarchical way, where each layer is a subgraph that consists of the edges with weights exceeding some threshold. We examine eleven real-world graphs from five different domains and observe consistently strong correlations between the number of common neighbors (CNs) of an edge and the weight of the edge. Although the information of CNs has been widely used in *link prediction* (Wang et al. 2015) and used to indicate the significance of *individual* edges (Ahmad et al. 2020; Cao et al. 2015; Zhu and Xia 2016), to the best of our knowledge, we are the first to study the *quantitative* patterns between the information of CNs and edge weights in a *macroscopic* scope. We observe consistent within-layer patterns in multiple layers: (1) the nearly-linear growth of fraction of high-weight edges with the number of CNs, (2) the relation between being adjacent and having high weights (specifically, the relation between the fraction of high-weight edges and that of adjacent pairs with the same name number of CNs), and across the layers, we observe a power-law correlation between the overall fraction of high-weight edges and the counterpart within the group of edges sharing no CNs. Based on the observations, we propose PEAR (**P**attern-based **E**dge-weight **A**ssignment on g**R**aphs), an algorithm for assigning realistic edge weights to a given topology by preserving all the observed macroscopic patterns. The proposed algorithm has only *two* parameters. On multiple real-world datasets, PEAR outperforms the baseline methods using the same number of, or even more, parameters, producing more realistic edge weights in several different aspects w.r.t different macroscopic network statistics.

In short, our contributions are five-fold:

- *New problem.* We introduce a new challenging problem: realistic assignment of edge weights *merely* based on *topology*.
- *New perspective.* We introduce the concept of *layers*, which provides a new perspective to study weighted graphs.
- *Patterns.* We extensively study eleven real-world graphs and discover the various relations between topology and edge weights.
- *Algorithm.* We propose PEAR, a weight-assignment algorithm based on the observed patterns. The algorithm has only *two* parameters yet produces realistic edge weights to a given topology.
- *Experiments.* We evaluate PEAR on real-world graphs. Without sophisticated fine-tuning, PEAR overall outperforms the baseline methods with more param-

[1] See Appendix E for some illustrative experiments, where we use edge weights generated by our proposed method to enhance the performance of a community detection method.

eters, producing more realistic edge-weights w.r.t node-degree and edge-CN distributions, average clustering coefficient, and a graph distance measure computed by NetSimile (Berlingerio et al. 2012).

Roadmap. The remaining part of the paper is organized as follows. In Sect. 2, we discuss related work. In Sect. 3, we provide some preliminaries. In Sect. 4, we propose some new concepts. In Sect. 5, we describe the patterns that we observe on real-world datasets. In Sect. 6, we formulate our observations and, based on them, propose our algorithm, PEAR. In Sect. 7, the empirical evaluation of PEAR on real-world datasets is demonstrated. In Sect. 8, we discuss some potential limitations of our work and future directions, and lastly, conclude the paper.
Reproducibility. The code and datasets are available at https://github.com/bokveizen/topology-edge-weight-interplay (Bu et al. 2022).

2 Related work

Edge-weight prediction. In the early trials of edge-weight prediction (Aicher et al. 2015; Zhao et al. 2015; Zhu et al. 2016), the problem is dealt with as a natural extension of the link prediction (Martínez et al. 2016) problem. Specifically, the proposed link-prediction algorithms assign scores to node pairs as the likelihood of edge existence, and the scores are also naturally used as the estimated edge weights. More recently, Fu et al. (2018) use multiple topological features to predict the unknown edge weights in a supervised manner. Specifically, they fit a regression model to the known edge weights with the features and use the fitted model to predict the unknown ones. The main differences between the problem that we focus on in this work and the edge-weight prediction problem are: (1) in the edge-weight prediction problem, most (e.g., 80% (Aicher et al. 2015) or 90% (Fu et al. 2018; Zhao et al. 2015; Zhu et al. 2016)) of the edge weights are assumed to be known and are given together with topology as the inputs, while we consider the scenarios where we only have access to the topology and we have *none* known edge weights; and (2) the target of the edge-weight prediction problem is to estimate the weights of individual edges in a *microscopic* way, while we aim to generate realistic edge weights for a given topology preserving the *macroscopic* patterns that we observe in real-world graphs. Notably, there is another independent research problem that focuses on the edge-weight prediction of weighted signed graphs, which has essential differences from the research problem in this paper. Specifically, the techniques proposed in a recent work studying that problem (Kumar et al. 2016) are specially designed for weighted signed graphs representing pairwise relations such as like/dislike and trust/distrust, which cannot be directly applied to the scenarios that we focus on where the edge weights represent the repetitions of the corresponding binary relations.
Weighted-graph generation. The other trials exploring the interplay between topology and edge weights, include the weighted-graph generation problem (Akoglu et al. 2008; McGlohon et al. 2008; Yang et al. 2021). In those works, the authors specifically study the evolution of both topology and edge weights over time, and they propose algorithms that generate both topology and edge weights of weighted graphs.

Although some simple static patterns (e.g., power-law or geometric weight distributions) are also discussed in those works, the problem that we focus on, generating edge weights for a given topology, is essentially and technically different with the weighted-graph generation problem since in our problem the topology is given and thus fixed.

Strong triadic closure. The concept of strong triadic closure (STC) is first proposed by Sintos and Tsaparas (2014), where the authors consider the problem of classifying edges into strong ones and weak ones. They define that a graph satisfies the STC property if there exists no open triangle with two strong edges,[2] and they assume that graphs often satisfy the STC property and have many strong edges. Therefore, they specifically consider the problem of maximizing the number of strong edges while satisfying the STC property. However, only two types of edge weights are considered in this problem, while real-world graphs often have a high diversity of edge weights (see, e.g., the datasets in Table 2). Moreover, this optimization problem has both theoretical (it can have many optimal solutions) and practical (real-world graphs often do not have many strong edges) limitations, as pointed out by Adriaens et al. (2020). Even though the above problem has been extended to edge weights of a wider range with other modifications (Adriaens et al. 2020), the extended version still has room for improvement w.r.t the empirical grounds, and the methods fail to predict the edge weights of real-world graphs accurately. Specifically, the predicted edge weights have almost zero correlation with the ground truth on many datasets, as shown by Adriaens et al. (2020).

To the best of our knowledge, we are the first to consider the problem of assigning realistic edge weights to a given topology by trying to preserve patterns observed on real-world graphs.

3 Preliminaries

In this section, we provide some mathematical and notational backgrounds.

A *weighted graph* $G = (V, E, W)$ consists of a node set $V = V(G)$, an edge set $E = E(G) \in \binom{V}{2}$, and edge weights $W = W(G)$. By ignoring the edge weights, we have the underlying *unweighted* graph $\overline{G} = (V, E)$ of G. For each edge $e \in E$, W_e is the *weight* of e. In this work, we focus on graphs with positive integer edge weights, i.e., $W \in \mathbb{N}^E$, where $\mathbb{N}$ is the set of positive integers, where each edge weight represents the number of occurrences of the corresponding edge. Note that the analysis on weighted graphs is mainly done on the graphs with integer edge weights (Newman 2004), and for graphs with non-integer edge weights, we may round each edge weight to the nearest integer. All graphs are assumed to be undirected and without self-loops. Thus, (u, v) and (v, u) represent the same edge (i.e., the set $\{u, v\}$) between two nodes $u \neq v \in V$.

[2] Formally, the STC property requires that, for any three nodes u, v, and w, if both of the edges (u, v) and (u, w) are strong, then the edge (v, w) must exist.

The concepts below use *only the topology* of G (i.e., V and E). For each node $v \in V$, $N_v(G) = \{v' \in V : (v, v') \in E\}$ is the *neighborhood* of v in G, and $d_v(G) = |N_v(G)|$ is the *degree* of v in G. For two nodes $u, v \in V$, $CN_{uv}(G) = N_u(G) \cap N_v(G)$ is the set of *common neighbors* (CNs) of u and v in G, and we say the two nodes u and v *share* the common neighbors in $CN_{uv}(G)$. For an edge $e = (u, v)$, we use $CN_e(G)$ to denote $CN_{uv}(G)$, and we say that the edge e *shares* the common neighbors in $CN_e(G)$. Sometimes, the number $|CN_e(G)|$ of common neighbors shared by the two endpoints of e is called the *embeddedness* (Cleaver 2002) of e.

Given $G = (V, E, W)$, the *line graph* (Harary and Norman 1960) of G is the graph $L(G) = (E, X)$, where the nodes of $L(G)$ one-to-one correspond to the edges of G and two nodes of $L(G)$ are adjacent to each other if and only if the two corresponding edges in G share a common endpoint. Given $k \in \mathbb{N}$, the k-core (Seidman 1983) $C_k(G)$ of G is the maximal subgraph of G where each node of $C_k(G)$ has degree k within it.

We list the frequently used notations and abbreviations in Table 1. In the notations, the input graph G can be omitted when the context is clear.

In this paper, we consider the problem where given the topology of a graph, we aim to assign realistic edge weights to the topology based on several patterns observed on real-world graphs, where each edge weight is a positive integer representing the number of occurrences of the corresponding edge. We formulate the considered problem (informally at this moment) as follows:

Problem 1 (Informal) Given an unweighted graph $\overline{G} = (V, E)$, we aim to generate edge weights $W : E \to \mathbb{N}$ that satisfy *a group of realistic properties regarding the interplay between topology and edge weights*, where each edge weight is a positive integer representing the number of occurrences of the corresponding edge.

We shall first present the patterns (i.e., the group of realistic properties) that we observe on real-world graphs, and then we provide a formal problem statement by formulating the patterns as mathematical properties. Finally, we propose an algorithm that assigns realistic edge weights to a given topology while preserving the formulated properties.

4 Proposed concepts

In this section, we introduce the proposed concepts. We will use them to describe our observations and design our algorithm.

When given an unweighted graph $\overline{G} = (V, E)$, the topology divides the pairs $\binom{V}{2}$ of nodes into two categories. Each pair $(u, v) \in \binom{V}{2}$ of nodes is either *adjacent* ($(u, v) \in E$, weight ≥ 1) or *distant* ($(u, v) \notin E$, weight < 1). When we have a weighted graph $G = (V, E, W)$, we can similarly set different weight thresholds $i \in \mathbb{N}$

Table 1 Notations and abbreviations

Notation/Abbreviation	Definition/Meaning
$G = (V, E, W)$	A graph with a node set V, a edge set E, and edge weights W
$\overline{G} = (V, E)$	The underlying unweighted graph of G
W_e	The edge weight of $e \in E$
$N_v(G)$	The set of neighbors of $v \in V$
$d_v(G)$	The degree of $v \in V$
$CN_{uv}(G)$	The set of common neighbors of $u, v \in V$
$G_i = (V_i, E_i, W_i)$	The layer-i of G whose edge set consists of the edges with weights $\geq i$ in G
$R_i = \binom{V_i}{2}$	The set of all the node pairs in G_i
$E_{c;i}(G)$	The set of edges sharing c common neighbors in G_i
$R_{c;i}(G)$	The set of pairs sharing c common neighbors in G_i
$f_{overall;i}(G)$ ($\tilde{f}_{overall;i}(G)$)	The overall fraction of weighty edges (adjacent pairs) w.r.t G and i (Def. 2)
$f_{c;i}(G)$ ($\tilde{f}_{c;i}(G)$)	The fraction of weighty edges (adjacent pairs) within $E_{c;i}(G)$ (Def. 2)
CN	Common neighbor
PEAR	**P**attern-based **E**dge-weight **A**ssignment on g**R**aphs
FoWE	Fraction of weighty edges
FoAP	Fraction of adjacent pairs

and extract the subgraph consisting of edges with weight $\geq i$, which gives the following definition of *layers*.

Definition 1 (Layers) Given $G = (V, E, W)$ and $i \in N$, the *layer-i* of G is the weighted graph $G_i = (V_i, E_i, W_i)$ obtained from G by taking the edges with weights greater than or equal to i.[3] Formally, $E_i = E_i(G) = \{e \in E : W_e \geq i\}$, and $W_i = W_i(G)$ satisfies that $W_i(e) = W(e), \forall e \in E_i$. We also define all the possible node pairs $R_i = R_i(G) = \binom{V_i}{2}$.

Based on the concept of layers, we also define the following related concepts, weighty edges (WEs) and fraction of weighty edges (FoWE), w.r.t each layer of a graph. Intuitively, in each layer, the weighty edges are the edges with weights higher than the threshold determined by the layer. Notably, we define overall FoWEs for the whole layer, and we also define FoWE w.r.t each number c of common neighbors (CNs).

Definition 2 (Fractions of weighty edges and adjacent pairs) Given $G = (V, E, W)$ and $i \in \mathbb{N}$, we call an edge $e \in E_i$ a *weighty edge* (w.r.t G and i) if and only if $W_e > i$ (i.e., $e \in E_{i+1}$), where recall that E_i is the edge set of G_i. The *overall*

[3] G_1, the layer-1 of G, is identical to the original graph G.

Table 2 Some basic statistics (number of nodes and number of edges in each of the first four layers) of the eleven real-world datasets (Opsahl 2013; Benson et al. 2018; Paranjape et al. 2017; Sinha et al. 2015) from five domains used in our empirical study. The datasets are grouped w.r.t their domains

Dataset	$\|V\|$	$\|E\| = \|E_1\|$	$\|E_2\|$	$\|E_3\|$	$\|E_4\|$
OF	897	71380	47,266 (66.2%)	35,456 (49.7%)	28,546 (40.0%)
FL	2905	15,645	4608 (29.5%)	1507 (9.6%)	564 (3.6%)
th-UB	82,075	182,648	7297 (4.0%)	2090 (1.1%)	965 (0.5%)
th-MA	152,702	1,088,735	128,400 (11.8%)	48,605 (4.5%)	26,121 (2.4%)
th-SO	2,301,070	20,989,078	1,168,210 (5.6%)	350,871 (1.7%)	170,618 (0.8%)
sx-UB	152,599	453,221	135,948 (30.0%)	56,115 (12.4%)	28,029 (6.2%)
sx-MA	24,668	187,939	74,493 (39.6%)	36,604 (19.5%)	21,364 (11.4%)
sx-SO	2,572,345	28,177,464	9,871,784 (35.0%)	4,137,454 (14.7%)	2,055,034 (7.3%)
sx-SU	189,191	712,870	216,296 (30.3%)	82,475 (11.6%)	37,655 (5.3%)
co-DB	1,654,109	7,713,116	2,269,679 (29.4%)	1,085,489 (14.1%)	654,182 (8.5%)
co-GE	898,648	4,891,112	1,055,077 (21.6%)	446,833 (9.1%)	246,944 (5.1%)

fraction of weighty edges $f_{overall;i}(G)$ is defined as $|E_{i+1}|/|E_i|$. Further given $c \in \mathbb{N}$, let $E_{c;i} \subseteq E_i$ denote the set of edges sharing c CNs (i.e., edges whose endpoints share c CNs) in G_i. The *fraction of weighty edges* (w.r.t G, i, and c) $f_{c;i}(G)$ is defined as $|E_{c;i} \cap E_{i+1}|/|E_{c;i}|$. Similarly, we define the *overall fraction of adjacent pairs* $\tilde{f}_{overall;i}(G) = |E_i|/|R_i|$, as well as the *fraction of adjacent pairs* (w.r.t G, i, and c) $\tilde{f}_{c;i}(G) = |E_{c;i}|/|R_{c;i}|$ for each c, where $R_{c;i}$ is the set of pairs sharing c CNs in G_i.[4]

5 Patterns in real-world graphs

In this section, we analyze eleven real-world graphs from different domains and extract patterns w.r.t the interplay between topology and edge weights.

Datasets We use 11 publicly-available real-world datasets from five different domains. In Table 2, we give some basic statistics (the number of nodes and the number of edges in each of the first four layers) of the datasets we study in this work. In all the datasets, the edge weights can be interpreted as the time of occurrences of the corresponding binary relation. We take the largest connected component of each graph. In the *OF* dataset (Opsahl 2013), the nodes are users and an edge represents communication within a blog post. In the *FL* (flights) dataset (Opsahl 2011), the nodes are airports and an edge represent a flight between two airports. In the *th* (threads) datasets (Benson et al. 2018), the nodes are users and an edge exists between two users if they participate in the same thread within 24 h. The *sx* (stack exchange) datasets (Paranjape

[4] Note that the fraction of adjacent pairs can be different from the *density* of the corresponding induced subgraph.

et al. 2017) are extracted from the same websites as the *th* datasets, but here an edge exists if one user answers or comments on a question of another, and the two groups of datasets are essentially different (see also Table 2 for the statistical difference). In the *co* (coauthorship) datasets (Benson et al. 2018; Sinha et al. 2015), the nodes are authors and an edge exists between the two authors if they coauthor a paper.

5.1 Why the number of common neighbors?

First, we shall show that the numbers of common neighbors (CNs) are consistently indicative of edge weights even when compared with the more complicated ones. We compare the numbers of CNs with several other quantities widely used in link prediction (Martínez et al. 2016) and edge-weight prediction (Fu et al. 2018). Notably, the number of CNs shared by two adjacent nodes is equal to the number of triangles involving the two nodes. Real-world graphs are rich in triangles (Tsourakakis 2008; Shin et al. 2020). For special graphs, e.g., bipartite graphs where no triangle exists, we can consider *butterflies* ((2, 2)-bicliques) instead (Sanei-Mehri et al. 2018).

Given a graph $G = (V, E, W)$, for each edge $(u, v) \in E$, we consider the following quantities, using only the topology (V and E):

- **NC (Number of common neighbors, also called *embeddedness*** (Cleaver 2002)). $NC_{uv} = |CN_{uv}|$.
- **SA (Salton index)** (Salton and McGill 1983). $SA_{uv} = NC_{uv}/\sqrt{d_u \cdot d_v}$.
- **JC (Jaccard index)** (Levandowsky and Winter 1971). $JC_{uv} = NC_{uv}/|N_u \cup N_v|$.
- **HP (Hub-promoted)** (Ravasz et al. 2002). $HP_{uv} = NC_{uv}/\min(d_u, d_v)$.
- **HD (Hub-depressed)** (Ravasz et al. 2002). $HD_{uv} = NC_{uv}/\max(d_u, d_v)$.
- **SI (Sørensen index)** (Sorensen 1948). $SI_{uv} = 2NC_{uv}/(d_u + d_v)$.
- **LI (Leicht-Holme-Newman index)** (Leicht et al. 2006). $LI_{uv} = NC_{uv}/(d_u \cdot d_v)$.
- **AA (Adamic-Adar index)** (Adamic and Adar 2003). $AA_{uv} = \sum_{x \in CN_{uv}} 1/\log d_x$.
- **RA (Resource allocation)** (Zhou et al. 2009). $RA_{uv} = \sum_{x \in CN_{uv}} 1/d_x$.
- **PA (Preferential attachment)** (Albert and Barabási 2002). $PA_{uv} = d_u \cdot d_v$.
- **FM (Friends-measure)** (Fire et al. 2011). $FM_{uv} = |\{(x \in N_u, y \in N_v) : x = y \vee (x, y) \in E\}| = NC_{uv} + |\{(x \in N_u, y \in N_v) : (x, y) \in E\}|$.
- **DL (Degree in the line graph)**. $DK_{uv} = d_u + d_v - 2$.
- **EC (Edge coreness)**. The maximum $k \in \mathbb{N}$ such that the edge (u, v) is in $C_k(G)$, the k-core (Seidman 1983) of G.
- **LP (Local path index)**. $LP_{uv} = (A^2)_{uv} + \epsilon(A^3)_{uv}$, where A is the adjacency matrix of G. We use $\epsilon = 10^{-3}$ as in (Zhou et al. 2009).

For each dataset and each considered quantity, we collect the sequence of the quantities of the edges and that of the binary indicators of repetition (i.e., having weight > 1), and compute the Point-biserial correlation coefficient (Tate 1954) between them.[5] In Table 3, we report the results. Among all the considered quantities, the

[5] The point-biserial correlation measures the correlation between a continuous variable and a discrete variable, and it is mathematically equivalent to the Pearson correlation.

number of CNs is the *simplest* one while having the *highest* average point-biserial correlation coefficient and the *highest* average ranking w.r.t the correlation with edge repetition over all the datasets. See Appendix B for the results measured by the area under the ROC curve (AUC).

For the four smallest datasets (OF, FL, sx-MA, and th-UB), we also use the four additional quantities with relatively high computational costs. They are (1) edge betweenness (Girvan and Newman 2002), (2) personalized pagerank (Jeh and Widom 2003), and two "node-centrality" measures in the line graph $L(G)$ (each node in $L(G)$ corresponds to an edge in G): (3) eigenvector centrality (Bonacich 1987) and (4) pagerank (Page et al. 1999). For all four datasets, NC consistently has a higher correlation than the four quantities mentioned above. Moreover, in line graphs, we also consider the closeness centrality (Freeman 1977), the betweenness centrality (Freeman 1977), and the clustering coefficients (Watts and Strogatz 1998). However, due to the even larger computational costs of these quantities, it is only possible to compute them on the smallest dataset *OF*, and the Pearson correlation coefficients are 0.12, 0.06, and -0.12 for the closeness centrality, the betweenness centrality, and the clustering coefficients, respectively, which are much lower than that of NC, even though they are much more complicated than NC.

Below, for the clarity and brevity of the presentation, we may visualize or report results on a small number of datasets, while similar results are obtained across all datasets. The full results on all the datasets are available in the supplementary material (Bu et al. 2022).

5.2 Observation 1: the fractions of weighty edges

We have shown that the numbers of CNs and the *repetition* (i.e., *weightiness* in layer-1) of edges are highly correlated. We examine this phenomenon in more layers and study the detailed numerical relations between the number c of CNs and the corresponding fraction of weighty edges (FoWE) $f_{c;i}$. In Fig. 1, for each dataset and each layer-i with $1 \leq i \leq 5$, we plot the FoWEs, where we can observe that the FoWEs grow *nearly linearly* with the number of CNs until some *saturation point* (see Definition 3) such that the FoWEs after the saturation point are almost 100%. In Fig. 1, we also show the results of the linear fitting for the points truncated before the corresponding saturation point with the R^2 values, where we can see consistently strong linear correlations. We formally define the *saturation point* of the fractions of weighty edges (FoWEs) as the minimum number c^* such that all the edges in $E_{c^*;i}$ are weighty edges.

Definition 3 (Saturation points of the fraction of weighty edges) Given G and i, the *saturation point* $c_i^*(G)$ of the fractions of weighty edges is defined as $\min\{c \in \mathbb{N} : f_{c;i} = 1\}$.

Table 3 The numbers of common neighbors are simple yet indicative

Dataset	NC	SA	JC	HP	HD	SI	LI	AA	RA	PA	FM	DL	EC	LP
OF	0.33	0.20	0.20	− 0.02	0.21	0.21	− 0.13	**0.34**	**0.35**	0.33	0.11	0.32	0.26	0.33
FL	0.32	0.26	0.26	0.19	0.24	0.26	− 0.06	**0.35**	**0.35**	0.21	0.08	0.18	0.17	0.31
th-UB	**0.48**	0.02	0.00	0.03	0.00	0.01	− 0.05	0.47	0.40	0.33	0.26	0.21	0.37	**0.48**
th-MA	**0.45**	0.22	0.15	0.09	0.15	0.18	− 0.05	0.44	0.35	0.33	0.40	0.25	0.38	**0.46**
th-SO	**0.38**	0.11	0.08	0.06	0.08	0.09	− 0.03	**0.39**	0.33	0.22	0.33	0.18	0.26	0.37
sx-UB	**0.15**	0.11	0.08	0.09	0.07	0.08	− 0.00	0.13	0.10	0.09	0.12	0.09	0.14	**0.15**
sx-MA	**0.25**	0.24	0.21	0.12	0.19	0.21	− 0.02	**0.25**	0.22	0.19	0.19	0.16	0.20	0.25
sx-SO	0.10	**0.11**	0.08	0.08	0.07	0.08	0.00	0.10	0.07	0.05	0.10	0.07	0.07	**0.10**
sx-SU	**0.14**	0.11	0.08	0.09	0.07	0.08	− 0.00	0.12	0.08	0.08	0.11	0.08	0.13	**0.15**
co-DB	**0.20**	− 0.08	− 0.09	− 0.05	− 0.08	− 0.08	− 0.16	**0.22**	0.20	0.03	0.06	0.07	0.14	0.20
co-GE	**0.30**	− 0.07	− 0.08	− 0.08	− 0.07	− 0.06	− 0.16	**0.32**	0.26	0.16	0.19	0.19	0.22	0.30
avg	**0.28**	0.11	0.09	0.05	0.09	0.10	− 0.06	**0.28**	0.24	0.18	0.18	0.16	0.21	0.28
avg. rank	**2.2**	7.5	10.5	10.6	10.8	8.9	14.0	2.5	5.5	8.2	7.1	8.5	6.5	**2.4**

We report the point-biserial correlation coefficients between the sequences of each quantity and the binary indicators of repetition. The two strongest correlations are highlighted in bold. See Appendix B for the results measured by the area under the ROC curve (AUC). Among all the considered quantities, the number of common neighbors is simplest while achieving the highest average rank in average over all the datasets

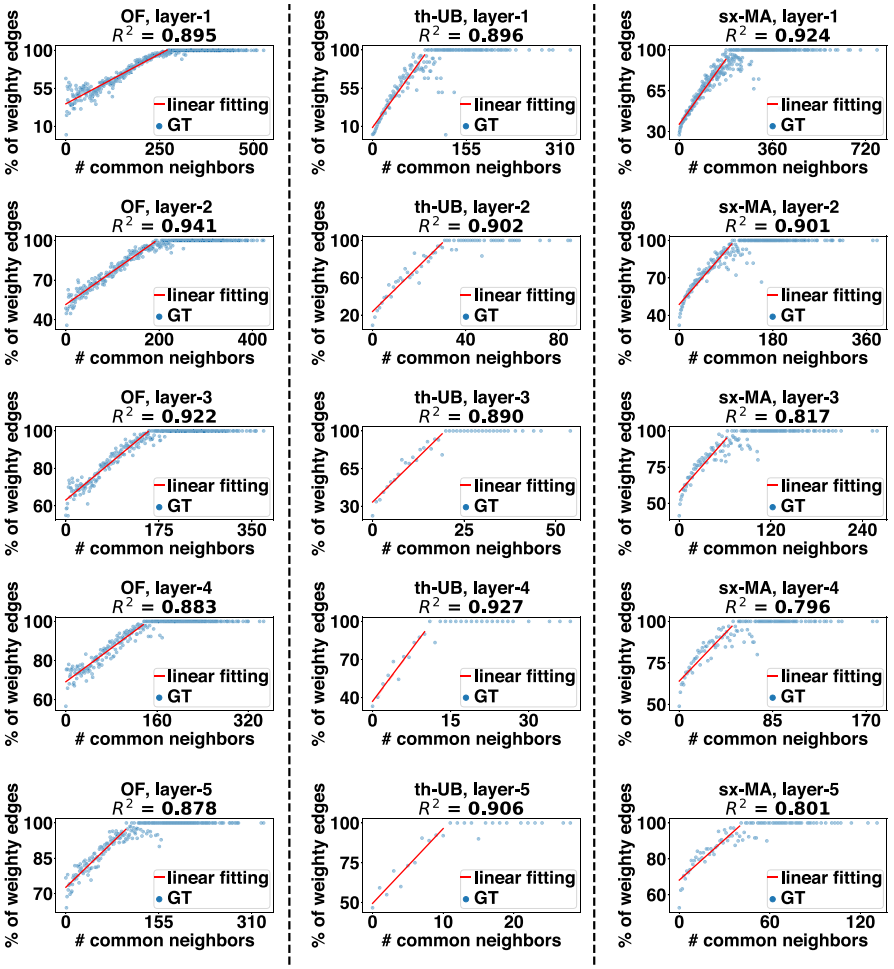

Fig. 1 Fractions of strong edges grow nearly linearly until a saturation point. We also report the R^2 of linear fitting before the saturation point. The R^2 is high in each layer, indicating that the growth is consistently nearly linear. See the supplementary material (Bu et al. 2022) for the full results

Remark 1 Theoretically, the above definition of saturation point may appear less robust since a single edge that is not weighty can affect the whole group of edges sharing the same number of CNs. We use such a definition for simplicity and clarity. In Appendix C, we discuss this issue and show the practical reasonableness of this definition on the datasets used in our empirical evaluation.

Observation 1 (Nearly linear growth of FoWEs) On each dataset, in each layer, the FoWEs grow nearly linearly with the number of CNs and become almost all 100% after some saturation point.

5.3 Observation 2: adjacency and weightiness

The number of CNs has been widely used for *link prediction* (Liu et al. 2011; Güneş et al. 2016), i.e., inferring the adjacency between node pairs. In the above Observation 1, we have shown the connection between the number of CNs and the weightiness of edges. Are the adjacency of pairs and the weightiness of edges also quantitatively related? In Fig. 2, for each dataset and each layer-i with $1 \leq i \leq 5$, we report how (a) the fraction of adjacent pairs within each group of pairs (i.e., $\tilde{f}_{c;i}$) and (b) the fraction of weighty edges within each group of edges (i.e., $f_{c;i}$) depend on the number of CNs, where consistently high Pearson correlation coefficients are observed. We summarize our observation w.r.t this similarity as follows.

As we have mentioned, the information of CNs has been used for link prediction (Wang et al. 2015) and for indicating the significance of individual edges (Ahmad et al. 2020; Cao et al. 2015; Zhu and Xia 2016), where the assumption is usually qualitative, e.g., node pairs between two nodes sharing more CNs are more likely to be adjacent (or more important). However, no existing works study the *quantitative* relation between the adjacency of pairs and the weightiness (repetition) of edges w.r.t the number of CNs in a unified way and compare them with each other.

Similar to the saturation point of FoWEs, we also defined the saturation point of the fractions of adjacent pairs (FoAPs) as the minimum number c^* such that all the pairs in $R_{c^*;i}$ are adjacent pairs.

Definition 4 (Saturation points of the fractions of adjacent pairs) Given G and i, recall that the *saturation point* $c_i^*(G)$ of the fractions of weighty edges is defined as $\min\{c \in \mathbb{N} : f_{c;i} = 1\}$, the *saturation point* $\tilde{c}_i^*(G)$ of the fractions of adjacent pairs is defined as $\min\{c \in \mathbb{N} : R_{c;i} = E_{c;i}\}$.

As shown in Table 4, we observe that the saturation point of the FoWEs is consistently similar to that of the FoAPs (see Fig. 2).

Observation 2 (Similarity between pair-adjacency and edge-weightiness) On each dataset, in each layer, the trends of the fractions of adjacent pairs and the fractions of weighty edges w.r.t the number of CNs have a high correlation (see the consistently high Pearson's r values),[6] and the saturation point of the FoWEs is close to that of the FoAPs.

5.4 Observation 3: a power law across layers

The previous observations describe some patterns within each layer. Is there any pattern that connects different layers? For each layer-i, we collect the information of $f_{0;i}$ (FoWE of the group of edges without CNs in layer-i) and $f_{overall;i}$ (the overall FoWE of all the edges in layer-i). By doing so, we obtain two sequences ($f_{0;i}$'s

[6] We are studying the correlations here, and the absolute differences are not necessarily small.

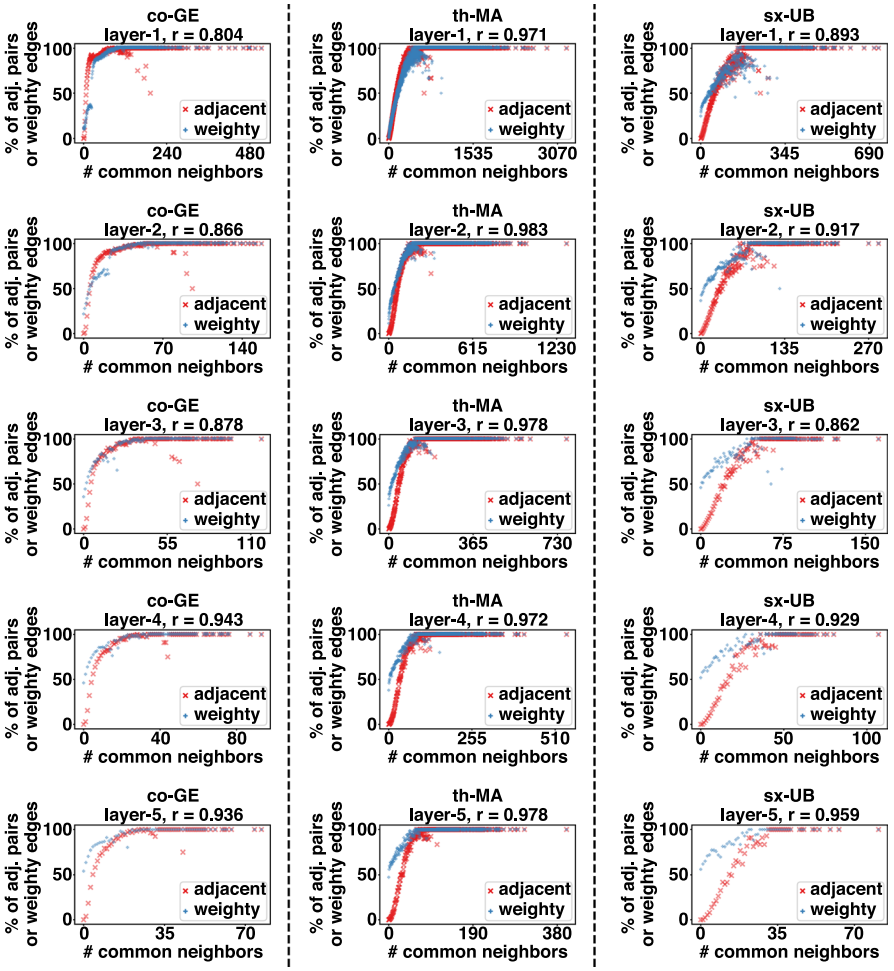

Fig. 2 The fractions of **a** adjacent pairs and **b** weighty edges within each group with the same number of common neighbors are similar. We report Pearson's r between the two fractions, which is high in each layer. Note that for each dataset, the range of the x-axis changes over layers, which is because the maximum number of common neighbors changes over layers. Also, we do not compare the fractions across different layers but only compare them within each layer. The full results are in the supplementary material (Bu et al. 2022)

and $f_{overall;i}$'s) across different layers. We observe a consistent and strong power law between the two sequences, which we visualize in Fig. 3. In the figure, for each dataset, we plot (a) the point $(f_{overall;i}, f_{0;i})$ for each $1 \leq i \leq 10$ in the log-log scale and (b) the power-law fitting line,[7] which is linear in the log-log scale. The consistent and strong power law is clearly observed.

[7] We only include the first four layers of *FL* since the layer-5 is too sparse and small.

Table 4 The saturation point of the fractions of weighty edges and that of the fractions of adjacent pairs are consistently close

Dataset	Layer-1	Layer-2	Layer-3	Layer-4	Layer-5
OF	241/271	190/192	157/156	134/137	119/101
FL	64/66	31/31	17/17	–	–
th-UB	73/87	30/31	19/20	18/11	15/11
th-MA	372/401	145/153	114/114	84/67	63/59
th-SO	685/750	208/205	134/129	97/82	74/72
sx-UB	152/149	63/69	48/42	36/27	31/22
sx-MA	185/181	113/102	75/63	60/49	51/41
sx-SO	886/749	407/324	221/203	169/130	120/103
sx-SU	202/206	96/93	63/54	48/37	36/27
co-DB	83/88	36/29	22/24	20/21	16/16
co-GE	74/92	52/49	34/40	28/30	24/21

For each layer of each dataset, we report the saturation point of the fractions of adjacent pairs on the left and that of the fractions of weighty edges on the right

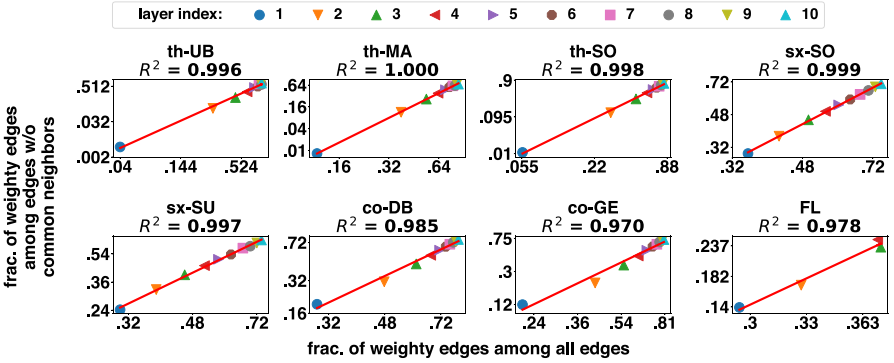

Fig. 3 Consistent and strong power laws exists between the fractions of weighty edges of **a** those without common neighbors and **b** those of all edges. We also report the R^2 of power-law fitting. The R^2 is consistently close to 1 for all datasets, indicating consistently strong power laws. See the supplementary material (Bu et al. 2022) for the full results

Observation 3 (A power law across layers) On each dataset, across the layers, the FoWEs of the group of edges sharing no CNs and the overall FoWEs of all edges follow a strong power law.

Remark 2 All the above observations are based on layer structures. For weighted graphs with positive-integer edge weights, decomposing such graphs into layers is straightforward, while for weighted graphs with real-valued edge weights, we can convert the edge weights into integers by rounding or other ways. Moreover, in the datasets used in this work, the edge weights represent the number of occurrences. Therefore, the observations may not hold on weighted graphs where the edge weights have other real-world meanings. See Appendix A for more discussions.

6 Proposed algorithm: PEAR

In this section, we propose PEAR (**P**attern-based **E**dge-weight **A**ssignment on g**R**aphs), an algorithm with only *two* parameters that assigns weights to a given topology. PEAR produces the edge weights layer by layer based on the above observations. Below, we shall describe the mathematical formulation of our observations and then the detailed procedure of PEAR.

6.1 Formulation of the observations

In Sect. 5, we describe the patterns that we have observed on the real-world datasets. For constructing an algorithm, we shall first mathematically formulate the observations. In the formulation, we may idealize the observations into simple, intuitive, and deterministic formulae.

Linear growth of FoWEs In Observation 1, we have mentioned that the fractions of weighty edges (FoWEs) grow *nearly linearly* with the number of CNs with some saturation points consistently over all datasets and all layers. In our algorithm PEAR, we assume *perfect linearity*, and we formulate this phenomenon as follows:

$$f_{c;i}(G) = \min(1, f_{0;i}(G) + (1 - f_{0;i}(G))\frac{c}{c_i^*(G)}), \forall G, i, c, \tag{1}$$

where $c_i^*(G)$ is the saturation point of FoWEs in G_i. By this formulation, $f_{c;i} = f_{0;i}$ when $c = 0$, and it increases with the number of CNs in a ratio of $(1 - f_{0;i})/c_i^*$ until $f_{c;i} = 1$ when c reaches c_i^* and stays with $f_{c;i} = 1$ thereafter.

Algorithm 1 PEAR for edge-weight assignment

Input: (1) $\overline{G} = (V, E)$, (2) power-law parameters a and k
Output: weight assignment W

$G_1 \leftarrow \overline{G}$
$W_e \leftarrow 1, \forall e \in E$
for $i = 1, 2, 3, \ldots$ **do**
  if $\tilde{c}_i^*$ does not exist or $\sum_{c<\tilde{c}_i^*} |E_{c;\,i}| = 0$ **then**
    Break
  end if
  $|E_{i+1}| \leftarrow$ the solution in $(0, |E_i|)$ of Equation (8) (Property (3))
  $f_{0;\,i} \leftarrow a(|E_{i+1}|/|E_i|)^k$ (Eq. (4))
  $c_i^* \leftarrow \tilde{c}_i^*$ (Property (2))
  $C_i \leftarrow \{|CN_e| : e \in E_i\}$
  $E_c \leftarrow \{e \in E_i : |CN_e| = c\}, \forall c \in C_i$
  $f_{c;\,i} \leftarrow \min(1, f_{0;\,i} + (1 - f_{0;\,i})c/c_i^*), \forall c \in C_i$ (Property (1))
  $E_{i+1} \leftarrow \emptyset$
  for each $c \in C_i$ **do**
    $\hat{E}_c \leftarrow$ sample $f_{c;\,i}|E_c|$ (rounded) edges in E_c uniformly at random
    $E_{i+1} \leftarrow E_{i+1} \cup \hat{E}_c$
  end for
  $W_e \leftarrow i + 1, \forall e \in E_{i+1}$
  $G_{i+1} \leftarrow (\bigcup_{e \in E_{i+1}} e, E_{i+1})$
end for
return W

Saturation points In Observations 2 and 1, we have mentioned the *similarity* between the trends of the fraction of adjacent pairs and the FoWEs and we have further pointed out that the saturation points of the two kinds of fractions are close. In the algorithm, we assume *equality* between $\tilde{c}_i^*$ and c_i^*, and we formulate it as follows:

$$c_i^*(G) = \tilde{c}_i^*(G), \forall G, i, \tag{2}$$

where recall that $\tilde{c}_i^*(G) = \min\{c : R_{c;i}(G) = E_{c;i}(G)\}$ and $R_{c;i}(G)$ is the set of node pairs sharing c CNs in G_i.

The power law across layers In Observation 3, we have mentioned that *the FoWEs of the group of edges sharing no CNs and the overall FoWEs of all edges follow a strong power law*. In the algorithm, assuming a *perfect* power law, we formulate it as follows:

$$f_{0;i}(G) = a(G) f_{overall;i}^{k(G)}, \forall G, i, \tag{3}$$

where $a(G)$ and $k(G)$ are the two parameters of the power law which may vary for each different graph G.

With Properties (1)–(3) formulated and explicitly described, we are now ready to re-state Problem 1 in a more formal and specific way.

Problem 2 (Formal) Given an unweighted graph $\overline{G} = (V, E)$, we aim to generate edge weights $W : E \to \mathbb{N}$ that satisfy Properties (1)–(3).

6.2 Algorithmic details

Now we are ready to describe the algorithmic details of PEAR (Algorithm 1), which combines all the above formulae to produce the edge weights layer by layer. From now on, we suppose that G is given as an input and thus fixed. By Equation (3) and the definition of $f_{overall;i} = |E_{i+1}/E_i|$, we have

$$f_{0;i} = a(|E_{i+1}|/|E_i|)^k, \forall i. \tag{4}$$

For each layer-i, the total number $|E_{i+1}|$ of weighty edges should be equal to the summation of the numbers of weighty edges in all the $E_{c;i}$'s. By Eqs. (1) and (2), it gives

$$\begin{aligned} |E_{i+1}| &= \sum_c |E_{c;i}| f_{c;i} = \sum_c |E_{c;i}| \min(1, f_{0;i} + (1 - f_{0;i})c/c_i^*) \\ &= \sum_c |E_{c;i}| \min(1, f_{0;i} + (1 - f_{0;i})c/\tilde{c}_i^*). \end{aligned} \tag{5}$$

Note that $\tilde{c}_i^*$ can be obtained from the given topology when $i = 1$ or from the currently generated layers when $i > 1$ (Line 9). We expand Eq. (5) to get

$$\begin{aligned} |E_{i+1}| &= \sum_{c \le \tilde{c}_i^*} |E_{c;i}|(f_{0;i} + (1 - f_{0;i})c/\tilde{c}_i^*) + \sum_{c > \tilde{c}_i^*} |E_{c;i}| \\ &= f_{0;i} \sum_{c \le \tilde{c}_i^*} |E_{c;i}|(\tilde{c}_i^* - c)/\tilde{c}_i^* + \sum_c |E_{c;i}| \min(1, c/\tilde{c}_i^*), \end{aligned} \tag{6}$$

which further gives the relation between $f_{0;i}$ and $\tilde{c}_i^*$:

$$f_{0;i} = \frac{|E_{i+1}| - \sum_c |E_{c;i}| \min(1, c/\tilde{c}_i^*)}{\sum_{c \le \tilde{c}_i^*} |E_{c;i}|(\tilde{c}_i^* - c)/\tilde{c}_i^*}. \tag{7}$$

Equations (4) and (7) give us two different expressions of $f_{0;i}$ and we can use them to obtain $|E_{i+1}|$ by solving the following equation:

$$a(|E_{i+1}|/|E_i|)^k = \frac{|E_{i+1}| - \sum_c |E_{c;i}| \min(1, c/\tilde{c}_i^*)}{\sum_{c < \tilde{c}_i^*} |E_{c;i}|(\tilde{c}_i^* - c)\tilde{c}_i^*}. \tag{8}$$

Remark 3 In Eq. (8), the denominator is zero only when $E_{c;i} = \emptyset$ for each $c \le \tilde{c}_i^*$, which implies that all the edges are strong edges and the generated edge weights are not meaningful.

Theorem 1 *Assume that* $\tilde{c}_i^* > 0$ *exists and* $\sum_{c<\tilde{c}_i^*} |E_{c;i}| > 0$. *If* $a < 1$ *and* $k > 1$, *then in the range* $(0, |E_i|)$, *Eq.* (8) *has a unique solution* $|E_{i+1}| \in (0, |E_i|)$.

Proof Define

$$g(x) = a(\frac{x}{|E_i|})^k - \frac{x - \sum_c |E_{c;i}| \min(1, c/\tilde{c}_i^*)}{\sum_{c\le\tilde{c}_i^*} |E_{c;i}|(\tilde{c}_i^* - c)\tilde{c}_i^*}$$

on $x \in [0, |E_i|]$. We have

$$g(0) = \frac{\sum_c |E_{c;i}| \min(1, c/\tilde{c}_i^*)}{\sum_{c\le\tilde{c}_i^*} |E_{c;i}|(\tilde{c}_i^* - c)\tilde{c}_i^*} > 0$$

and $g(|E_i|) = a - 1 < 0$. Since f is continuous, by the intermediate value theorem (see also Bolzano's theorem), we have at least one solution in the range $(0, |E_i|)$. For the uniqueness, we have

$$f''(x) = ak(k-1)x^{k-2}/|E_i|^k > 0, \forall x \in (0, |E_i|)$$

(i.e., f is convex on $(0, |E_i|)$). Assume that we have two roots $0 < x_1 < x_2 < |E_i|$, let $t = (|E_i| - x_2)/(|E_i| - x_1) \in (0, 1)$, then by the convexity of f we have

$$0 = g(x_2) = g(tx_1 + (1-t)|E_i|) \le tg(x_1) + (1-t)g(|E_i|) = (1-t)g(|E_i|) < 0,$$

completing the proof by contradiction. □

After obtaining $|E_{i+1}|$ (Line 7), we use Eq. (4) to compute $f_{0;i}$ (Line 8), and then use Eq. (1) with $c_i^* = \tilde{c}_i^*$ to compute all $f_{c;i}$'s (Lines 9 and 12). Then for each c, we sample $f_{c;i}|E_c|$ edges uniformly at random in E_c in the current layer G_i to be weighty edges, assign the edge weights accordingly, and construct the next layer G_{i+1} (Lines 13–19). We repeat the process layer after layer. By Theorem 1, if we have a valid saturation point $\tilde{c}_i^*$ and there exist edges sharing less than $\tilde{c}_i^*$ CNs, we can always obtain a unique solution of $|E_{i+1}|$ from Eq. (8), and thus the whole process can continue. If any of the conditions are not met, the process terminates, and the current edge weights are returned as the final output (Lines 4 and 21).

The following theorem shows the time complexity of Algorithm 1.

Theorem 2 *Given an input graph* $\overline{G} = (V, E)$ *and two parameters* a *and* k, *Algorithm* 1 *takes* $O(i_{max} \sum_{v\in V} d_v^2))$ *time to output a weight assignment* W, *where* i_{max} *is the maximum layer index such that* $G_{i_{max}}$ *is non-empty*, *i.e.*, *the maximum weight in the output*.

Proof We shall show that it takes $O(\sum_{v\in V} d_v^2)$ to generate each layer. The time complexity consists of (1) that of computing $\tilde{c}_i^*$ (Line 9) and (2) that of sampling weighty edges (Lines 14–17). For (1), checking the CNs of all pairs can be done by enumerating all neighbor pairs of each node, which takes $O(\sum_{v\in V} d_v^2(G_i)) = O(\sum_{v\in V} d_v^2(G))$

time. For (2), sampling among E_i takes $O(|E_i|) = O(|E|) = O(\sum_{v \in V} d_v(G))$ time, completing the proof. □

The following theorem states that Algorithm 1 indeed preserves all the formulated properties and is What are the relations between the edge weights and the topology in real-world graphs? Given only the topology of a graph, how can we assign realistic weights to its edges based on the relations? Several trials have been done for *edge-weight prediction* where some unknown edge weights are predicted with most edge weights known. There are also existing works on generating both topology and edge weights of weighted graphs. Differently, we are interested in generating edge weights that are realistic in a macroscopic scope, merely from the topology, which is unexplored and challenging. To this end, we explore and exploit the patterns involving edge weights and topology in real-world graphs. Specifically, we divide each graph into *layers* where each layer consists of the edges with weights at least a threshold. We observe consistent and surprising patterns appearing in multiple layers: the similarity between being adjacent and having high weights, and the nearly-linear growth of the fraction of edges having high weights with the number of common neighbors. We also observe a power-law pattern that connects the layers. Based on the observations, we propose PEAR, an algorithm assigning realistic edge weights to a given topology. The algorithm relies on only *two* parameters, preserves *all* the observed patterns, and produces more realistic weights than the baseline methods with the same number of, or even more, parameters. a valid approach for Problem 2.

Theorem 3 *Given any* $\bar{G} = (V, E)$, a, *and* k, *the output of PEAR* (*Algorithm* 1) *satisfies Properties* (1)–(3) *up to integer rounding*.

Proof Property (1) is explicitly preserved by Line 12, and Property (2) is explicitly preserved by Line 9. Regarding Property (3), since Property (1) is preserved, the solution of Equation (8) which combines Properties (1) and (3) preserves Property (3), completing the proof. □

Remark 4 Due to the interconnectedness of all the three properties, for any fixed a and k, the output of PEAR is unique up to the sampling (Line 14-17), which is evidentially supported by the small standard variations in Tables 5 and 6.

7 Experiments

In this section, through experiments on the real-world graphs, we shall show that, in most cases, PEAR generates realistic edge weights for a given topology with only *two* parameters and *without sophisticated searching or fine-tuning* on the parameters.

Table 5 PEAR generates more realistic edge weights than the baseline methods in terms of KSCN and KSND

metric	method	OF	FL	th-UB	th-MA	th-SO	sx-UB	sx-MA	sx-SO	sx-SU	co-DB	co-GE	AVG	A.R
KSCN	PRD	0.542	0.522	0.722	0.840	0.768	0.242	0.486	0.259	0.299	0.656	0.731	0.55	8.36
	SCN	0.485	0.661	0.528	0.579	0.634	0.782	0.681	0.795	0.768	0.661	0.573	0.65	8.18
	SEB-R	0.217	0.401	0.712	0.773	0.737	0.252	0.362	0.305	0.328	0.484	0.488	0.46	7.00
	SEB-N	0.475	**0.184**	0.670	0.601	0.624	0.100	0.221	0.159	0.237	0.155	0.199	0.33	3.73
	PEB-R	0.626	0.368	0.665	0.711	0.607	0.109	0.310	**0.137**	0.154	0.529	0.577	0.44	4.82
	PEB-N	0.626	0.368	0.665	0.711	0.607	0.109	0.310	**0.137**	0.154	0.529	0.577	0.44	4.82
	STC	0.679	0.474	0.705	0.772	0.698	0.292	0.707	0.380	0.362	0.238	0.419	0.52	7.82
	RFF	0.265	0.236	0.346	0.368	0.434	0.805	0.560	0.734	0.713	0.293	0.131	0.44	5.36
	NEB-R	0.147	0.339	0.719	0.899	0.559	0.274	0.416	0.304	0.364	**0.096**	**0.085**	0.38	5.45
	NEB-N	0.140	FAIL	FAIL	0.901	0.732	0.304	0.749	**0.137**	0.277	0.224	0.383	FAIL	7.09
	PEAR **(ours)**	**0.074±0.003**	0.241±0.017	**0.168±0.015**	**0.186±0.006**	**0.126±0.008**	**0.076±0.003**	**0.072±0.001**	0.239±0.001	**0.103±0.002**	0.329±0.013	0.181±0.008	**0.16**	**2.18**
KSND	PRD	0.096	0.164	0.336	0.219	0.161	0.040	**0.059**	**0.027**	0.045	0.237	0.292	0.15	4.36
	SCN	0.359	0.424	0.406	0.587	0.443	0.544	0.556	0.371	0.506	0.311	0.283	0.44	9.91
	SEB-R	0.087	0.180	0.361	0.201	0.157	0.038	0.067	0.038	0.057	0.231	0.289	0.16	4.64
	SEB-N	0.096	0.121	0.336	0.212	0.155	**0.027**	0.065	0.034	0.041	0.155	0.198	0.13	3.09
	PEB-R	0.232	0.172	0.289	0.248	0.133	0.041	0.085	0.071	0.057	0.274	0.293	0.17	5.27
	PEB-N	0.232	0.172	0.289	0.248	0.133	0.042	0.085	0.071	0.057	0.274	0.294	0.17	5.45
	STC	0.577	0.385	0.452	0.441	0.397	0.303	0.492	0.531	0.354	0.306	0.374	0.42	10.00
	RFF	0.115	0.146	0.267	0.388	0.322	0.602	0.416	0.246	0.410	0.217	0.121	0.30	6.64
	NEB-R	0.148	0.108	0.389	0.430	0.326	0.128	0.163	0.346	0.194	**0.055**	0.113	0.22	6.18
	NEB-N	0.085	FAIL	FAIL	0.327	0.352	0.229	0.247	0.208	0.165	0.090	0.284	FAIL	7.09
	PEAR **(ours)**	**0.069±0.002**	**0.070±0.002**	**0.157±0.009**	**0.175±0.009**	**0.129±0.002**	**0.027±0.000**	0.146±0.001	0.178±0.003	**0.022±0.000**	0.105±0.007	**0.105±0.001**	**0.11**	**2.09**

For each dataset and each metric, we report the average over the layers generated by each method, as well as the average (AVG) over all datasets and the average rank (A.R.), where the best result is in **bold**, and the second-best one is underlined (OOM = out of memory; FAIL = unable to output a meaningful layer). See Appendix G for the full results

Table 6 PEAR generates more realistic edge weights than the baseline methods in terms of DACC and NetSimile

metric	method	OF	FL	th-UB	th-MA	th-SO	sx-UB	sx-MA	sx-SO	sx-SU	co-DB	co-GE	AVG	A.R
DACC	PRD	0.291	0.184	0.239	0.371	0.211	0.036	0.139	0.036	0.047	0.370	0.376	0.21	8.45
	SCN	0.166	0.417	0.434	0.457	0.486	0.587	0.523	0.520	0.589	0.160	0.129	0.41	9.00
	SEB-R	0.060	0.135	0.235	0.356	0.204	0.035	0.118	0.036	0.048	0.271	0.213	0.16	6.55
	SEB-N	0.246	**0.036**	0.215	0.311	0.190	0.018	0.102	0.026	0.039	0.054	0.046	0.12	3.55
	PEB-R	0.240	0.131	0.225	0.313	0.190	0.023	0.064	**0.024**	0.018	0.344	0.341	0.17	4.64
	PEB-N	0.240	0.131	0.225	0.313	0.190	0.023	0.063	**0.024**	**0.017**	0.344	0.341	0.17	4.45
	STC	**0.027**	0.077	0.231	0.273	0.155	0.036	0.148	0.036	0.046	0.117	0.205	0.12	4.55
	RFF	0.187	0.106	0.279	0.418	0.399	0.645	0.468	0.548	0.595	0.197	0.120	0.36	8.36
	NEB-R	0.126	0.142	0.237	0.377	0.162	0.032	0.103	**0.024**	0.049	**0.051**	0.037	0.12	4.73
	NEB-N	0.028	FAIL	FAIL	0.378	0.195	0.042	0.173	0.030	0.031	0.087	0.175	FAIL	6.91
	PEAR **(ours)**	0.158±0.006	0.080±0.007	**0.129±0.004**	**0.262±0.001**	**0.146±0.001**	**0.016±0.000**	**0.043±0.000**	0.037±0.000	0.023±0.001	0.227±0.005	0.127±0.004	**0.11**	**3.27**
	PRD	11.99	16.81	24.71	23.80	22.38	15.33	12.49	OOM	15.39	19.83	19.93	18.27	7.10
	SCN	15.47	20.56	18.68	21.76	23.39	24.89	22.77	OOM	25.45	12.62	13.32	19.89	7.30
	SEB-R	9.34	16.26	25.15	23.70	21.32	16.46	12.06	OOM	17.38	17.74	17.64	17.71	6.20
	SEB-N	10.67	12.29	24.52	23.29	22.77	8.51	**8.91**	OOM	12.85	16.06	17.34	15.72	4.30
	PEB-R	12.03	14.11	19.28	19.40	17.45	13.04	12.81	OOM	13.65	18.51	17.55	15.78	4.90
	PEB-N	12.02	14.12	19.29	19.40	17.45	13.05	12.80	OOM	13.65	18.49	17.55	15.78	5.00
	STC	23.57	21.16	27.70	26.03	23.08	24.04	25.53	OOM	25.08	21.35	22.27	23.98	10.00
	RFF	12.26	13.81	16.51	18.10	18.96	25.61	20.87	OOM	25.42	**14.71**	7.54	17.38	5.30
	NEB-R	11.10	12.95	21.31	22.88	20.49	17.11	14.20	OOM	19.27	**9.73**	8.89	15.79	4.90
	NEB-N	**6.21**	FAIL	FAIL	26.69	22.96	29.80	27.12	OOM	22.49	19.52	21.79	FAIL	9.20
	PEAR **(ours)**	8.09±0.32	**8.92±0.17**	**9.33±0.22**	**14.85±0.07**	**13.79±0.10**	**6.03±0.12**	9.40±0.04	OOM	**6.37±0.14**	15.73±0.24	10.87±0.04	**10.34**	**1.70**

For each dataset and each metric, we report the average over the layers generated by each method, as well as the average (AVG) over all datasets and the average rank (A.R.), where the best result is in **bold**, and the second-best one is underlined (OOM = out of memory; FAIL = unable to output a meaningful layer). See Appendix G for the full results

7.1 Baseline methods and experimental settings

The following baseline methods (PRD, SCN, SEB, PEB, and STC) are *unsupervised* in that they do not use any explicit ground truth edge-weight information. However, for these methods to output meaningful predictions, we provide the ground-truth number of edges for each layer-i (i.e., $|E_i|$) with $2 \leq i \leq 5$ to them. Such *additional* information is *not* provided to PEAR.[8]

- *PRD (purely random)* The PRD method repeatedly uniformly at random chooses an edge and increments its weight until the $|E_i|$'s are satisfied.
- *SCN (sorting-CN)* Instead of random sampling, the SCN method sorts the edges by the number of CNs and assigns the weights accordingly (higher weights to the edges with more CNs).[9]
- *SEB (sorting-embedding)* The SEB method sorts the edges by the inner product of the node embeddings of the two endpoints of each edge and assigns higher weights to the edges with higher inner products. The node embeddings are produced by two different methods, RandNE (Zhang et al. 2018; Rozemberczki et al. 2020) and node2vec (Grover and Leskovec 2016). We use SEB-R and SEB-N to denote the results using RandNE and node2vec, respectively. The feature dimension is set as 32, and all the other parameters are kept the same as in the original paper.
- *PEB (probability-embedding)* The PEB method uses node embeddings as in SEB, and it repeatedly chooses an edge and increments its weight until the $|E_i|$'s are satisfied, where the exponential of the inner product of the node embeddings of the two endpoints of each edge is used as the weight of the edge in the sampling. We use PEB-R and PEB-N to denote the results using RandNE and node2vec, respectively.
- *STC (strong triadic closure)* The STC method makes use of the strong triadic closure (Sintos and Tsaparas 2014) (STC) principle. Specifically, for each layer-i, the STC method first uses a greedy algorithm to maximize the number of candidate weighty edges in the layer without having any open triangle (i.e., three nodes v_1, v_2, v_3 s.t. the two edges (v_1, v_2) and (v_1, v_3) exist and (v_2, v_3) does not exist). After that, the STC method uniformly at random samples $|E_i|$ weighty edges among all the candidates.[10]

[8] The $|E_i|$'s (specifically, $|E_1|$, $|E_2|$, $|E_3|$, and $|E_4|$) are essentially *four* parameters, compared to only *two* parameters used in PEAR.

[9] The CNs are counted in each original graph (i.e., layer-i) instead of in each layer. An optimization problem in (Adriaens et al. 2020) of maximizing the total edge weights of all triangles is equivalent to this method.

[10] We simply take all the candidates, if $|E_i|$ is larger than the number of candidates. We have also tried including all the candidates as the weighty edges, which, however, for each dataset, produced layers that only change slightly after layer-2, and thus cannot produce meaningful edge weights more than binary categorization.

By contrast, for the proposed method PEAR, we only consider *two* settings $(a, k) \in \{(0.98, 1.02), (0.7, 1.3)\}$, where for the two *co* datasets and the four *sx* datasets we use $(a, k) = (0.98, 1.02)$; and for the remaining datasets we use $(a, k) = (0.7, 1.3)$. For each dataset, we report the results in the better setting. Note that these settings are chosen without relying on ground-truth weights. Specifically, when we choose the parameters, we simply move two parameters a and k in the opposite directions, while keeping $a + k = 2$, so that all the candidate parameter settings satisfy the assumptions in Theorem 1. Also, the best-performing settings show clear domain-based patterns. Specifically, we can use the same parameter setting for datasets in the same domain. Although it is challenging to find the best-performing setting for a dataset merely based on its topology,[11] the structural similarity between datasets within the same real-world domain (Chakrabarti and Faloutsos 2006; Wills and Meyer 2020) can be utilized to find a proper setting for each dataset based on the topology. See Appendix D for more discussions.

We also consider two *supervised* edge-weight prediction methods directly supervised by ground-truth edge weights. Notably, the supervised methods deal with the prediction task as a classification task and do not rely on the layer structure. We give the below supervised methods 10% of the ground truth edge weights as the input training set (and another 10% as the validation set if needed). We make sure each of the training set covers all five classes: edges of weight $1, 2, 3, 4, \geq 5$, corresponding to the five layers we are studying. Notably, the supervised methods use much more parameters. The considered methods are:

- *RFF (random forest-feature)* The RFF method uses a random forest classifier (Breiman 2001) with the 14 metrics we have used in Sect. 5.1 (see Table 3), which follows the procedure in a previous work (Fu et al. 2018) except for that the random forest is smaller and some metrics are not used due to its high computational cost as mentioned in Sect. 5.1. The hyperparameters of random forest are listed as follows: the number of trees = 32, the maximum depth of the tree = 5, and all the other parameters are kept the same as in the original work (Breiman 2001).
- *NEB (neural network-embedding)* The NEB method uses a neural network consisting of one bilinear layer. For each edge, the node embeddings of both endpoints, which are obtained as in SEB, are used as the input, and the neural network is trained to minimize a classification loss (cross-entropy). We use NEB-R and NEB-N to denote the results using RandNE and node2vec, respectively.

[11] As a weighted graph evolves, its topology may stay the same, but the edge weights representing the repetitions of edges may change. Such scenarios imply that for a given topology, multiple optimal groups of edge weights exist, and thus it is hard to find the best-performing setting.

7.2 Evaluation methods

We would re-emphasize that we aim to generate edge weights that are realistic in a *macroscopic* scope, and thus the evaluation should also be in a macroscopic scope. We report the following metrics including several graph statistics that have been widely used for evaluating graph generators (Leskovec et al. 2005; Shuai et al. 2013; Cao et al. 2015; Heath and Parikh 2011) to compare, for each $2 \leq i \leq 5$, the layer-i produced by each method and the original one: (1) KS statistic for number-of-CN distributions **(KSCN)**, (2) KS statistic for node-degree distributions **(KSND)**, (3) difference in average clustering coefficients **(DACC)**, and (4) a graph distance measure computed by **NetSimile** (Berlingerio et al. 2012).[12] The intuition is that if two weighted graphs have similar layers with the same layer index, then the two weighted graphs are similar too. Note that the evaluation focuses on the first four layers since, for $i > 5$, the ground-truth layer-i is too small or too sparse in some datasets. See Appendix F for more analysis using graph motifs.

7.3 Results

First, we show how the methods perform on each dataset. In Tables 5 and 6, for each dataset, each metric, and each method, we report the average value over all the generated layers. For PEAR, the mean value and the standard deviation over three trials of each setting are reported. Overall, PEAR has the best average value and the highest average rank among all the methods w.r.t each metric. Specifically, PEAR achieves an average rank of 2.18, 2.09, 3.27, and 1.70 (there are 11 methods in total), w.r.t the metric KSCN, KSNC, DACC, and NetSimile, respectively. Notably, although supervised with some ground-truth edge weights, the supervised baseline methods do not show clear superiority over the unsupervised ones. In our understanding, this is because the edge-weight classes (i.e., layers) are highly imbalanced (i.e., the numbers of edges with different weights vary a lot), while the ground-truth numbers of edges in each edge-weight class are provided to the unsupervised baseline methods including SEB are helpful. Also, the methods using sophisticated embeddings are sometimes even worse than SCN which assigns edge weights using a simple heuristic based on the number of CNs. In our understanding, this is because local information is important (according to our observations), while the embedding-based methods focus on higher-order information which can be confusing and harmful to the prediction results.

In Fig. 4, for the two datasets *th-UB* and *sx-MA*, and for $i \in \{2, 3, 4\}$, we report the node-degree and edge-CN distributions of the layer-i generated by each method, where the layers generated by PEAR have the two distributions closest to the

[12] Given a graph, NetSimile uses seven node-level structural features to generate a characteristic vector for the graph after feature aggregation over the nodes. Notably, we do not need to solve the node-correspondence problem for NetSimile and the measure is size-invariant (Berlingerio et al. 2012). NetSimile runs out of memory on *sx-SO* and the corresponding results are unavailable.

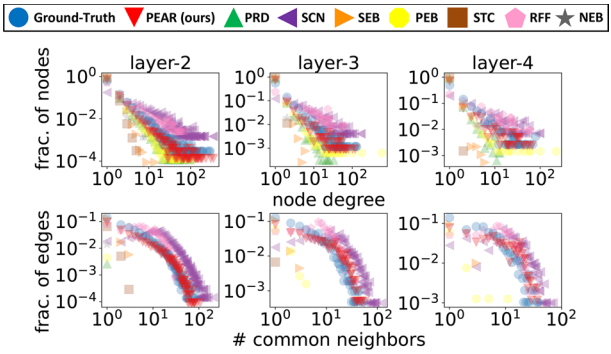

(a) *threads-ubuntu*, $(a, k) = (0.7, 1.3)$

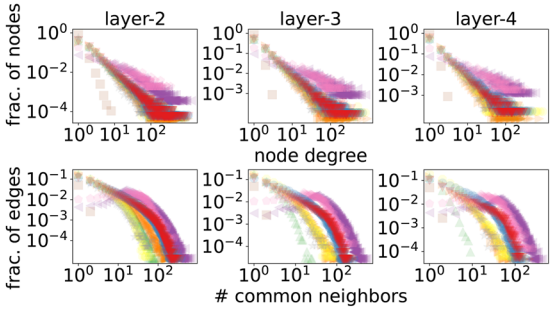

(b) *sx-math*, $(a, k) = (0.98, 1.02)$

Fig. 4 PEAR produces realistic edge weight. For each $i \in \{2, 3, 4\}$ and each method including the ground truth, we report the node-degree and number-of-CN distributions of the generated layer-i. See Tables 5 and 6 for the numerical comparison in detail

original ones. For each baseline method using embeddings, between the two variants using RandNE and node2vec, we report the results of the variant that performs better.

We also study how the performance varies across generated layers. In Fig. 5, for each method, each metric, and each layer index i, we report the average over all datasets. Again, for each baseline method using embeddings, between the two variants using RandNE and node2vec, we report the results of the variant that performs better. Overall, PEAR performs best for each layer.

8 Conclusion and future directions

In this work, we explored the relations between edge weights and topology in real-world graphs. We proposed a new concept called layers (Definition 1) with several related concepts (Definition 2), and observed several pervasive patterns (Observations 2–3). We also proposed PEAR (Algorithm 1), a weight-assignment algorithm with only two parameters, based on the formulation of our observations (Properties (1)–(3) and Eqs. (4)–(8)). In our experiments on eleven real-world graphs, we

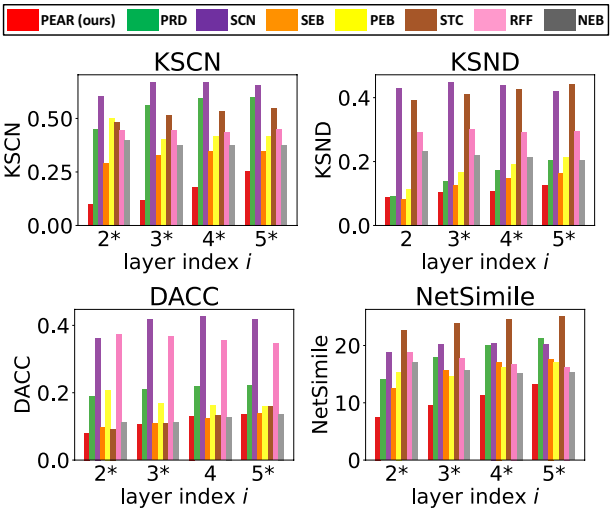

Fig. 5 PEAR generates edge weights that are realistic in each layer. For each generated layer-i with $i \in \{2, 3, 4, 5\}$, each method, and each metric, we report the average over all datasets. We use asterisk marks ($*$) to indicate the 14 (out of 16) cases where PEAR performs best. See Tables 5 and 6 for the numerical comparison in detail

showed that PEAR generates more realistic edge weights than the baseline methods, including those requiring much more prior knowledge and parameters (Tables 5 and 6 and Figs. 4 and 5).

The observations in this work are macroscopic and the proposed model is based on those observations. Although macroscopic patterns are relatively more robust to outliers compared to microscopic ones, it is still possible that outliers can impair the performance of our method. We plan to explore and examine how outliers can affect the performance of our method and the corresponding solutions. We studied weighted graphs with positive-integer edge weights, and we plan to extend the study on the interplay between edge weights and topology to real-valued edge weights. We studied the average behavior of each group of edges or pairs with the same number of common neighbors, and we plan to further explore the patterns within each group. We also plan to study how the two parameters of PEAR affect the output.

A General edge weights

As mentioned in Remark 2, all the observations in this work are based on layer structures, and the edge weights are limited to integer ones representing the number of occurrences. In order to examine the generality of our observations and the proposed algorithm, we examined several blockchain transaction datasets (Kılıç et al. 2022a, 2022), where each edge weight is a real number representing the amount of the corresponding transaction. On the transaction datasets mentioned above, the correlations between the edge weights and the number of common

neighbors are very low (consistently less than 0.1). Therefore, our observations and the proposed algorithm can not be directly applied to these datasets, which is a limitation of this work.

For general weighted graphs, we may make use of the known observation that real-world weighted graphs often have a heavy-tailed edge-weight distribution (Barrat et al. 2004; Kumar et al. 2020; Starnini et al. 2017). We leave as a potential future direction the exploration of the relation between edge weights and the number of common neighbors on weighted graphs with more general edge weights, as well as weighted graphs with edge weights having different real-world meanings (other than the number of occurrences).

B The indicativeness of the number of common neighbors

In Sect. 5.1, we have compared the indicativeness of the number of common neighbors with some baseline quantities measured by the point-biserial correlation coefficients (which are mathematically equivalent to the Pearson correlation coefficients). We would like to also examine this relation using other metrics, e.g., the area under the ROC curve (AUC).

In Table 7, we report the additional results measured by the AUC. Specifically, for each quantity, we first perform logistic regression between the sequence of the quantity and the binary indicators of repetition, then we compute the AUC of the output prediction. Although there are some baseline quantities achieving marginally higher AUC values, the number of common neighbors is still one of the most promising quantities, especially when we consider its simplicity.

C Saturation points

In Definition 4, we have defined the saturation point of the fraction of weighty edges (adjacent pairs) as the number c of common neighbors such that all (i.e., 100%) the edges (pairs) sharing c common neighbors are weighty (adjacent). Theoretically, this definition can be less robust since a single edge (pair) that is not weighty (adjacent) can affect the whole group of edges (pairs) sharing the same number of common neighbors. We have chosen to use the current definition for simplicity and clarity, while it is possible to make the concept more robust by using a less "absolute" threshold, e.g., "99%".

In Table 8, we show how the saturation points in the datasets used in our experiments change when we change the "100%" in the definition to "99%". In the real-world datasets that we use, such a change makes no big difference. Therefore, we claim that such a simple and clear definition is expected to work well in practice, but practitioners may take the issue discussed above into consideration for better robustness.

Table 7 The numbers of common neighbors are simple yet indicative. Additional results: we report the area under the ROC curve (AUC) of the logistic regression fit to the sequences of each quantity and the binary indicators of repetition

Dataset	NC	SA	JC	HP	HD	SI	LI	AA	RA	PA	FM	DL	EC	LP
OF	0.704	0.636	0.641	0.508	0.637	0.641	0.632	0.707	0.723	0.705	0.571	0.692	0.666	0.704
FL	0.676	0.664	0.657	0.619	0.647	0.657	0.479	0.698	0.725	0.629	0.546	0.606	0.610	0.674
th-UB	0.890	0.689	0.702	0.590	0.704	0.702	0.499	0.879	0.832	0.122	0.805	0.781	0.872	0.895
th-MA	0.843	0.751	0.701	0.587	0.689	0.701	0.662	0.845	0.823	0.834	0.800	0.741	0.801	0.844
th-SO	0.831	0.717	0.687	0.646	0.676	0.687	0.580	0.837	0.808	0.199	0.796	0.756	0.768	0.827
sx-UB	0.586	0.579	0.576	0.565	0.575	0.576	0.446	0.585	0.581	0.592	0.582	0.576	0.577	0.598
sx-MA	0.635	0.631	0.613	0.574	0.606	0.613	0.506	0.639	0.645	0.623	0.605	0.595	0.611	0.634
sx-SO	0.562	0.561	0.551	0.560	0.549	0.551	0.463	0.563	0.566	0.553	0.555	0.552	0.538	0.563
sx-SU	0.588	0.576	0.570	0.570	0.569	0.570	0.455	0.587	0.583	0.593	0.585	0.580	0.578	0.596
co-DB	0.624	0.529	0.523	0.530	0.521	0.523	0.587	0.617	0.586	0.360	0.624	0.627	0.601	0.630
co-GE	0.684	0.527	0.512	0.551	0.505	0.512	0.616	0.687	0.633	0.679	0.654	0.658	0.651	0.686
avg	0.693	0.624	0.612	0.573	0.607	0.612	0.539	0.695	0.682	0.535	0.648	0.651	0.661	0.696
avg. rank	3.00	8.18	9.18	11.18	11.18	9.18	12.45	2.45	4.18	7.27	7.36	7.73	7.73	2.27

Table 8 The saturation point of the fractions of adjacent pairs does not change much when we change the threshold in the definition from 100% to 99%

Dataset	Layer-1	Layer-2	Layer-3	Layer-4	Layer-5
OF	241/234	190/190	157/157	134/134	119/119
FL	64/64	31/31	17/17	–	–
th-UB	73/73	30/30	19/19	18/18	15/15
th-MA	372/372	145/145	114/114	84/84	63/63
th-SO	685/685	208/208	134/134	97/97	74/74
sx-UB	152/152	63/63	48/48	36/36	31/31
sx-MA	185/185	113/113	75/75	60/60	51/51
sx-SO	886/886	407/407	221/221	169/169	120/120
sx-SU	202/202	96/96	63/63	48/48	36/36
co-DB	83/83	36/20	22/17	20/17	16/14
co-GE	74/74	52/46	34/32	28/27	24/22

For each layer of each dataset, we report the saturation point of the fractions of adjacent pairs with threshold 100% on the left and the saturation point with threshold 99% on the right

D Parameters

As discussed in Sect. 7, PEAR uses only two parameters (a and k), and for the eleven real-world datasets used in our experiments, we only use *two* parameter settings $(a, k) \in \{(0.98, 1.02), (0.7, 1.3)\}$ without fitting to the ground-truth edge weight.

In Table 9, we report the results on the *parameter sensitivity* of PEAR, where we provide the performance of PEAR with four different parameter settings (including the two considered parameter settings $(a, k) \in \{(0.98, 1.02), (0.7, 1.3)\}$). In the table, for each parameter setting, we also report the average rank of PEAR (as in Tables 5 and 6) if we use the setting for PEAR.

One observed limitation of PEAR is its considerable *parameter sensitivity*. That is, using PEAR with different parameters can give fairly different performances. Therefore, it is important to find a well-working group of parameters when using PEAR.

First, we would like to emphasize that finding the best parameters is not a trivial problem. This is because, for a given topology, multiple plausible groups of edge weights are possible (consider, e.g., multiple snapshots of an evolving weighted graph).

Fortunately, PEAR works well without extensive parameter searching (specifically, only with two parameter settings) in the form of $(1 - x, 1 + x)$, and we have observed that for datasets within the same domain, we can use the same parameter setting. Notably, even simply using the same parameters $(a, k) = (0.98, 1.02)$, PEAR still achieves the best average value for each metric (compare the values in Tables 5, 6, and 9).

Another interesting and insightful observation is that the well-performing parameters of the datasets are seemingly correlated to the correlation between the numbers of common neighbors and the repetition of edges. Based on the point-biserial correlation coefficients between the sequences of the numbers of

Table 9 The parameter sensitivity results of PEAR

	KSCN		KSND		DACC		NetSimile	
Metric								
Dataset	(0.98, 1.02)	(0.7, 1.3)	(0.98, 1.02)	(0.7, 1.3)	(0.98, 1.02)	(0.7, 1.3)	(0.98, 1.02)	(0.7, 1.3)
OF	0.391±0.002	0.074±0.003	0.254±0.000	0.069±0.002	0.057±0.001	0.158±0.006	12.754±0.038	8.087±0.320
FL	0.425±0.001	0.241±0.017	0.159±0.002	0.070±0.002	0.141±0.003	0.080±0.007	16.563±0.063	8.918±0.171
th-UB	0.482±0.002	0.168±0.015	0.188±0.002	0.157±0.009	0.187±0.001	0.129±0.004	18.661±0.031	9.327±0.224
th-MA	0.239±0.003	0.186±0.006	0.071±0.001	0.175±0.000	0.151±0.003	0.262±0.001	15.680±0.028	14.854±0.074
th-SO	0.544±0.001	0.126±0.008	0.109±0.002	0.129±0.002	0.189±0.000	0.146±0.001	18.698±0.069	13.786±0.098
sx-UB	0.076±0.003	0.416±0.003	0.027±0.000	0.118±0.010	0.016±0.000	0.071±0.004	6.026±0.115	17.414±0.094
sx-MA	0.072±0.001	0.176±0.009	0.146±0.001	0.098±0.003	0.043±0.000	0.059±0.000	9.397±0.041	11.684±0.084
sx-SO	0.239±0.001	0.315±0.004	0.178±0.003	0.202±0.001	0.037±0.000	0.038±0.001	N/A	N/A
sx-SU	0.103±0.002	0.376±0.000	0.022±0.000	0.116±0.005	0.023±0.001	0.057±0.003	6.366±0.144	17.237±0.112
co-DB	0.329±0.013	N/A	0.105±0.007	N/A	0.227±0.005	N/A	15.731±0.236	N/A
co-GE	0.181±0.008	0.431±0.009	0.105±0.001	0.375±0.005	0.127±0.004	0.341±0.001	10.871±0.038	17.722±0.056
AVG	0.280	0.287	0.124	0.178	0.109	0.157	13.075	14.306
A.R	3.09	4.45	3.09	4.64	3.64	5.27	3.30	3.90
Dataset	(0.9, 1.1)	(0.5, 1.5)	(0.9, 1.1)	(0.5, 1.5)	(0.9, 1.1)	(0.5, 1.5)	(0.9, 1.1)	(0.5, 1.5)
OF	0.247±0.005	0.105±0.004	0.177±0.003	0.144±0.003	0.030±0.001	0.185±0.001	10.471±0.404	9.617±0.075
FL	0.212±0.012	0.323±0.007	0.056±0.005	0.107±0.010	0.054±0.010	0.086±0.009	12.116±0.062	11.626±0.231
th-UB	0.375±0.002	0.221±0.007	0.269±0.005	0.093±0.007	0.212±0.001	0.043±0.003	17.422±0.089	9.637±0.028
th-MA	0.350±0.002	0.222±0.011	0.184±0.001	0.099±0.001	0.305±0.001	0.158±0.001	15.438±0.140	14.418±0.092
th-SO	0.393±0.003	0.152±0.004	0.206±0.001	0.082±0.002	0.199±0.000	0.071±0.002	17.851±0.090	13.295±0.049
sx-UB	0.141±0.003	0.526±0.008	0.108±0.001	0.209±0.011	0.016±0.000	0.176±0.011	13.209±0.099	19.761±0.501
sx-MA	0.153±0.000	0.266±0.004	0.071±0.002	0.106±0.004	0.090±0.000	0.072±0.002	6.167±0.147	14.421±0.134
sx-SO	0.143±0.002	0.428±0.001	0.297±0.001	0.143±0.001	0.030±0.001	0.098±0.003	N/A	N/A
sx-SU	0.135±0.002	0.492±0.003	0.137±0.002	0.180±0.004	0.027±0.000	0.158±0.011	13.521±0.123	19.791±0.260
co-DB	N/A	N/A	N/A	N/A	N/A	N/A	N/A	N/A

Table 9 (continued)

	KSCN		KSND		DACC		NetSimile	
co-GE	0.486±0.001	0.464±0.003	0.386±0.000	0.288±0.005	0.344±0.000	0.299±0.004	17.732±0.023	17.244±0.080
AVG	0.299	0.336	0.214	0.162	0.154	0.151	14.775	15.211
A.R	3.18	4.45	5.73	4.82	4.36	5.27	3.60	4.30

We report the performance of PEAR with four different parameter settings on the eleven real-world datasets used in our experiments, with the average rank of PEAR among all the baseline methods and PEAR for each parameter

common neighbors and the binary indicators of repetition in Table 3, we can see that for all the datasets with a high coefficient (specifically, larger than 0.30), the parameter setting $(a, k) = (0.7, 1.3)$ performs better than $(a, k) = (0.98, 1.02)$, while for all the dataset with a relatively low coefficient, the situation is the opposite. Although the repetition of edges cannot be directly obtained merely from the topology, this provides insights into the reasons why PEAR with different parameters shows different performance on different datasets. We leave finding optimal parameters of PEAR for a given topology as a future direction.

E An application: community detection

As mentioned in the introduction (Sect. 1), assigning realistic edge weights to a given topology is an important and practical problem, and the predicted edge weights output by PEAR can be used in many practical applications. Here, we showcase one possible application, where we use the predicted edge weights to enhance the performance of community detection algorithms on graphs.

We use seven datasets with ground-truth clusters but without groud-truth edge weights, including (1–2) citation networks *cora* and *citeseer* (Sen et al. 2008), (3–5) website networks *cornell*, *texas*, and *wisconsin* (Pei et al. 2020), and (6–7) co-purchasing networks *computer* and *photo* (Shchur et al. 2018).[13]

For each dataset, we compare the performance of the Louvain method (Blondel et al. 2008) on the original unweighted graph and on the weighted counterpart with edge weights predicted by PEAR. For simplicity, we only predict a single layer, i.e., layer-2. The parameter settings (a, k) used on the datasets are: (0.95, 1.05) for *cora*; (0.99, 1.01) for *citeseer*, *pubmed*, *computer*, and *photo*; and (0.9, 1.1) for *cornell*, *texas*, and *wisconsin*. We then measure the performance w.r.t the adjusted rand index (ARI) and the normalized mutual information (NMI).

See Table 10 for the detailed results, where we can observe that the predicted edge weights consistently improve the community detection performance of the Louvain method, and we leave further exploration of this application (e.g., the reasons behind this improvement) as a future direction. In our understanding, the edge weights output by PEAR reinforce the local structures and thus enhance the performance. Indeed, triangle counts have been shown to be a helpful feature for community detection (Satuluri et al. 2011; Tsourakakis et al. 2017; Benson et al. 2016). Even on weighted graphs with ground-truth edge weights, one can still use PEAR to obtain another group of edge weights and use the edge weights predicted by PEAR as additional features.

[13] More details of these datasets can be found at https://pytorch-geometric.readthedocs.io/en/latest/notes/data_cheatsheet.html (Fey and Lenssen 2019).

Table 10 The predicted edge weights output by PEAR can enhance the community detection performance of the Louvain method

Dataset	ARI (unweighted)	ARI (PEAR)	NMI (unweighted)	NMI (PEAR)
cora	0.2481 ± 0.0189	$\mathbf{0.2507 \pm 0.0151}$	0.4546 ± 0.0069	$\mathbf{0.4570 \pm 0.0055}$
citeseer	0.0937 ± 0.0069	$\mathbf{0.0950 \pm 0.0059}$	0.3287 ± 0.0027	$\mathbf{0.3292 \pm 0.0020}$
pubmed	0.0946 ± 0.0034	$\mathbf{0.0948 \pm 0.0083}$	0.1774 ± 0.0033	$\mathbf{0.1779 \pm 0.0035}$
computer	0.3147 ± 0.0119	$\mathbf{0.3201 \pm 0.0199}$	0.5411 ± 0.0083	$\mathbf{0.5459 \pm 0.0056}$
photo	0.5696 ± 0.0301	$\mathbf{0.5796 \pm 0.0074}$	0.6673 ± 0.0165	$\mathbf{0.6722 \pm 0.0069}$
cornell	0.0230 ± 0.0006	$\mathbf{0.0274 \pm 0.0011}$	0.0956 ± 0.0019	$\mathbf{0.1014 \pm 0.0030}$
texas	0.0513 ± 0.0025	$\mathbf{0.0758 \pm 0.0007}$	0.0698 ± 0.0014	$\mathbf{0.0835 \pm 0.0030}$
wisconsin	0.0230 ± 0.0039	$\mathbf{0.0290 \pm 0.0045}$	0.0911 ± 0.0057	$\mathbf{0.0977 \pm 0.0047}$

For seven real-world datasets, we report the community detection performance of the Louvain method on the original unweighted graph and the weighted counterpart with edge weighted output by PEAR. The performance is measured by adjusted rand index (ARI) and normalized mutual information (NMI). The better results are marked in bold

F Evaluation using graph motifs

In this section, we provide the additional results where we evaluate predicted edge weights by analyzing graph motifs in each layer. Specifically, for each dataset, and for each $2 \leq i \leq 5$, we compare the layer-i output by each method, by counting the number of different 3-motifs (induced subgraphs of size 3, up to graph isomorphism) and comparing the distributions. There are three kinds of (nonempty) 3-motifs (up to graph isomorphism): (1) a single edge and an isolated node, (2) a wedge (i.e., an open triangle), and (3) a (closed) triangle. In each output layer, we iterate all the 3-subgraphs and count the 3-motifs. Then we use their ratios to obtain a sum-one vector of size 3 for each case. The final performance is measured by the L1 difference (which is equivalent to the total variance (Garner and McGill 1956)) between the distribution in the original graph and that in the output one. This comparison is related to the difference in average clustering coefficients in that both comparisons involve triangles, but the evaluation using graph motifs provides a different perspective, focusing more on the local patterns. For brevity, we only report the results of PEAR and SEB-N, which perform consistently better than the other method. See Table 11 for the detailed results, where in most cases PEAR shows better performance.

G Full experimental results

In this section, we show the full results of our experiments which we cannot put all in the main text due to the space limit. In Tables 12, 13, 14, 15, 16, 17, 18, 19, 20, 21 and 22, for each dataset, we report the detailed results w.r.t each metric, each method, and each layer. For the three methods using embeddings (i.e., SEB, PEB, and NEB), we use a "-R" suffix to denote the results using RandNE and we use a "-N" suffix to denote the results using node2vec.

Table 11 Evaluation using graph motifs. For each dataset, and for each $2 \leq i \leq 5$, we compare the layer-i output by each method, by counting the number of different 3-motifs (induced subgraphs of size 3, up to graph isomorphism) and comparing the distributions (i.e., vectors of size 3)

Dataset	Layer-2		Layer-3		Layer-4		Layer-5	
Method	SEB*	PEAR	SEB*	PEAR	SEB*	PEAR	SEB*	PEAR
OF	6.26E-2	**1.05E-2**	1.11E-1	**1.30E-2**	1.41E-1	**4.44E-2**	1.57E-1	**6.40E-2**
FL	1.57E-2	**3.38E-3**	2.51E-2	**6.27E-3**	3.46E-2	**1.37E-2**	4.59E-2	**2.54E-2**
th-UB	2.89E-2	**1.82E-2**	6.88E-2	**3.09E-2**	1.14E-1	**4.00E-2**	1.55E-1	**3.20E-2**
th-MA	3.09E-2	**2.12E-2**	5.47E-2	**3.19E-2**	7.30E-2	**3.46E-2**	8.71E-2	**2.90E-2**
th-SO	2.48E-3	**7.30E-4**	4.75E-3	**3.84E-3**	**6.61E-3**	1.55E-2	**8.07E-3**	3.21E-2
sx-UB	2.09E-3	**1.10E-4**	3.24E-3	**2.85E-3**	**3.74E-3**	6.76E-3	**3.71E-3**	1.15E-2
sx-MA	6.06E-3	**2.13E-3**	1.11E-2	**5.41E-3**	1.54E-2	**7.49E-3**	1.95E-2	**9.20E-3**
sx-SO	2.52E-4	**4.99E-5**	3.73E-4	9.10E-4	**4.49E-4**	2.50E-3	**5.39E-4**	4.56E-3
sx-SU	2.81E-3	**1.19E-3**	5.04E-3	**5.65E-4**	7.38E-3	**3.01E-3**	1.00E-2	**5.38E-3**
co-DB	4.56E-5	**7.72E-6**	5.59E-5	**1.19E-5**	6.15E-5	**1.69E-5**	6.59E-5	**2.23E-5**
co-GE	1.26E-4	**4.84E-5**	1.65E-4	**8.43E-5**	1.92E-4	**1.13E-4**	2.16E-4	**1.40E-4**

The final performance is measured by the L1 difference (which is equivalent to the total variance) between the distribution in the original graph and that in the output one. The better results (i.e., smaller errors) are marked in bold. Note that SEB* uses the ground-truth number of edges in each layer

Table 12 Full experimental results on *th-UB*

Metric	Method	Layer-2	Layer-3	Layer-4	Layer-5
KSCN	PRD	0.619	0.715	0.763	0.790
	SCN	0.595	0.547	0.526	0.443
	SEB-R	0.607	0.708	0.756	0.779
	SEB-N	0.533	0.657	0.720	0.769
	PEB-R	0.620	0.614	0.730	0.697
	PEB-N	0.620	0.614	0.730	0.697
	STC	0.556	0.710	0.763	0.790
	RFF	0.313	0.369	0.352	0.351
	NEB-R	0.609	0.715	0.763	0.790
	NEB-N	0.538	0.715	N/A	N/A
	PEAR **(ours)**	0.190±0.005	0.116±0.017	0.168±0.017	0.200±0.027
KSND	PRD	0.196	0.298	0.389	0.459
	SCN	0.473	0.472	0.350	0.328
	SEB-R	0.204	0.321	0.419	0.502
	SEB-N	0.189	0.302	0.389	0.462
	PEB-R	0.199	0.247	0.316	0.394
	PEB-N	0.198	0.247	0.316	0.394
	STC	0.305	0.433	0.506	0.562
	RFF	0.144	0.350	0.298	0.275
	NEB-R	0.270	0.375	0.443	0.469
	NEB-N	0.156	0.241	N/A	N/A
	PEAR **(ours)**	0.121±0.004	0.174±0.006	0.182±0.013	0.150±0.018
DACC	PRD	0.143	0.209	0.276	0.328
	SCN	0.496	0.489	0.399	0.352
	SEB-R	0.138	0.206	0.273	0.323
	SEB-N	0.104	0.184	0.257	0.317
	PEB-R	0.143	0.188	0.269	0.299
	PEB-N	0.143	0.188	0.269	0.299
	STC	0.113	0.206	0.276	0.328
	RFF	0.138	0.374	0.330	0.273
	NEB-R	0.136	0.209	0.276	0.328
	NEB-N	0.083	0.209	0.276	0.328
	PEAR **(ours)**	0.102±0.001	0.124±0.002	0.150±0.009	0.142±0.010

Table 12 (continued)

Metric	Method	Layer-2	Layer-3	Layer-4	Layer-5
NetSimile	PRD	20.959	23.523	26.813	27.562
	SCN	21.034	20.132	18.238	15.326
	SEB-R	20.630	24.608	27.174	28.192
	SEB-N	20.339	23.964	26.151	27.629
	PEB-R	20.878	19.689	19.127	17.424
	PEB-N	20.911	19.689	19.127	17.424
	STC	22.044	26.734	31.114	30.920
	RFF	17.313	18.154	15.549	15.041
	NEB-R	22.501	20.131	20.839	21.778
	NEB-N	20.989	28.706	N/A	N/A
	PEAR **(ours)**	10.116±0.352	9.210±0.211	9.318±0.281	8.665±0.629

Table 13 Full experimental results on *th-MA*

Metric	Method	Layer-2	Layer-3	Layer-4	Layer-5
KSCN	PRD	0.730	0.848	0.887	0.895
	SCN	0.580	0.591	0.577	0.568
	SEB-R	0.661	0.783	0.815	0.833
	SEB-N	0.544	0.609	0.622	0.627
	PEB-R	0.739	0.690	0.694	0.721
	PEB-N	0.739	0.691	0.694	0.721
	STC	0.753	0.768	0.766	0.801
	RFF	0.342	0.339	0.374	0.415
	NEB-R	0.887	0.903	0.905	0.902
	NEB-N	0.892	0.903	0.905	0.902
	PEAR **(ours)**	0.166±0.000	0.144±0.002	0.179±0.010	0.255±0.017
KSND	PRD	0.133	0.205	0.259	0.280
	SCN	0.595	0.597	0.590	0.564
	SEB-R	0.117	0.193	0.236	0.258
	SEB-N	0.128	0.198	0.248	0.272
	PEB-R	0.139	0.246	0.288	0.320
	PEB-N	0.139	0.246	0.288	0.320
	STC	0.411	0.432	0.449	0.471
	RFF	0.405	0.390	0.383	0.373
	NEB-R	0.424	0.425	0.442	0.431
	NEB-N	0.277	0.318	0.358	0.354
	PEAR **(ours)**	0.137±0.002	0.188±0.004	0.204±0.004	0.170±0.003

Table 13 (continued)

Metric	Method	Layer-2	Layer-3	Layer-4	Layer-5
DACC	PRD	0.303	0.369	0.403	0.409
	SCN	0.467	0.467	0.452	0.441
	SEB-R	0.278	0.353	0.393	0.401
	SEB-N	0.240	0.310	0.343	0.352
	PEB-R	0.305	0.312	0.322	0.312
	PEB-N	0.305	0.312	0.322	0.312
	STC	0.205	0.256	0.286	0.344
	RFF	0.473	0.421	0.391	0.386
	NEB-R	0.321	0.374	0.404	0.410
	NEB-N	0.322	0.374	0.404	0.410
	PEAR **(ours)**	0.215±0.001	0.279±0.002	0.290±0.002	0.263±0.004
NetSimile	PRD	19.974	24.147	25.210	25.857
	SCN	21.198	22.229	21.980	21.634
	SEB-R	19.708	24.016	25.192	25.887
	SEB-N	19.442	23.695	24.717	25.304
	PEB-R	20.277	18.374	18.806	20.125
	PEB-N	20.267	18.383	18.806	20.125
	STC	24.551	26.088	26.563	26.915
	RFF	19.096	17.926	17.502	17.892
	NEB-R	24.681	21.923	22.156	22.753
	NEB-N	27.871	26.918	26.250	25.712
	PEAR **(ours)**	10.106±0.037	14.945±0.199	16.894±0.092	17.473±0.081

Table 14 Full experimental results on *th-SO*

Metric	Method	Layer-2	Layer-3	Llayer-4	Layer-5
KSCN	PRD	0.704	0.776	0.792	0.800
	SCN	0.649	0.646	0.629	0.613
	SEB-R	0.637	0.744	0.775	0.790
	SEB-N	0.554	0.636	0.654	0.651
	PEB-R	0.706	0.541	0.571	0.612
	PEB-N	0.706	0.541	0.571	0.612
	STC	0.580	0.666	0.758	0.787
	RFF	0.451	0.421	0.425	0.439
	NEB-R	0.474	0.579	0.571	0.614
	NEB-N	0.704	0.734	0.743	0.748
	PEAR **(ours)**	0.188±0.001	0.119±0.002	0.077±0.008	0.121±0.022
KSND	PRD	0.070	0.139	0.194	0.241
	SCN	0.451	0.458	0.435	0.427
	SEB-R	0.074	0.142	0.185	0.228
	SEB-N	0.075	0.137	0.185	0.223
	PEB-R	0.072	0.127	0.146	0.187
	PEB-N	0.072	0.127	0.146	0.187
	STC	0.338	0.364	0.427	0.457
	RFF	0.312	0.327	0.327	0.320
	NEB-R	0.329	0.322	0.321	0.331
	NEB-N	0.360	0.347	0.348	0.353
	PEAR **(ours)**	0.112±0.000	0.167±0.001	0.135±0.005	0.101±0.005
DACC	PRD	0.149	0.205	0.235	0.257
	SCN	0.527	0.505	0.464	0.450
	SEB-R	0.131	0.198	0.231	0.254
	SEB-N	0.122	0.184	0.216	0.238
	PEB-R	0.149	0.180	0.206	0.227
	PEB-N	0.149	0.180	0.206	0.227
	STC	0.011	0.141	0.218	0.250
	RFF	0.459	0.406	0.376	0.354
	NEB-R	0.092	0.155	0.181	0.218
	NEB-N	0.137	0.189	0.216	0.237
	PEAR **(ours)**	0.123±0.000	0.156±0.001	0.157±0.003	0.148±0.004

Table 14 (continued)

Metric	Method	Layer-2	Layer-3	Llayer-4	Layer-5
NetSimile	PRD	20.562	22.485	23.102	23.385
	SCN	23.646	23.821	23.439	22.666
	SEB-R	19.271	21.319	22.086	22.608
	SEB-N	19.641	22.903	24.093	24.435
	PEB-R	20.544	13.841	15.926	19.471
	PEB-N	20.563	13.843	15.925	19.472
	STC	22.020	21.292	23.244	25.772
	RFF	20.500	18.956	18.409	17.991
	NEB-R	22.043	20.275	19.527	20.103
	NEB-N	24.565	23.259	22.315	21.710
	PEAR **(ours)**	11.215±0.032	13.121±0.035	14.569±0.204	16.239±0.168

Table 15 Full experimental results on *sx-UB*

metric	method	layer-2	layer-3	layer-4	layer-5
KSCN	PRD	0.194	0.250	0.263	0.262
	SCN	0.673	0.792	0.828	0.833
	SEB-R	0.231	0.262	0.257	0.257
	SEB-N	0.095	0.039	0.103	0.164
	PEB-R	0.220	0.079	0.068	0.068
	PEB-N	0.221	0.079	0.068	0.068
	STC	0.351	0.288	0.267	0.263
	RFF	0.789	0.806	0.813	0.810
	NEB-R	0.315	0.269	0.252	0.258
	NEB-N	0.367	0.304	0.278	0.267
	PEAR **(ours)**	0.027±0.001	0.068±0.005	0.098±0.006	0.110±0.004
KSND	PRD	0.021	0.036	0.050	0.054
	SCN	0.382	0.548	0.610	0.635
	SEB-R	0.021	0.038	0.044	0.050
	SEB-N	0.026	0.035	0.032	0.016
	PEB-R	0.032	0.072	0.047	0.014
	PEB-N	0.033	0.073	0.046	0.015
	STC	0.388	0.313	0.271	0.242
	RFF	0.558	0.594	0.620	0.635
	NEB-R	0.161	0.125	0.116	0.109
	NEB-N	0.220	0.172	0.278	0.246
	PEAR **(ours)**	0.049±0.000	0.013±0.005	0.016±0.003	0.027±0.002

Table 15 (continued)

metric	method	layer-2	layer-3	layer-4	layer-5
DACC	PRD	0.040	0.037	0.034	0.031
	SCN	0.442	0.589	0.642	0.673
	SEB-R	0.042	0.036	0.032	0.030
	SEB-N	0.026	0.021	0.016	0.009
	PEB-R	0.044	0.004	0.012	0.032
	PEB-N	0.044	0.004	0.012	0.032
	STC	0.050	0.034	0.030	0.029
	RFF	0.628	0.645	0.651	0.655
	NEB-R	0.042	0.032	0.027	0.028
	NEB-N	0.058	0.042	0.035	0.032
	PEAR **(ours)**	0.005±0.000	0.015±0.001	0.021±0.000	0.022±0.001
NetSimile	PRD	9.225	14.532	17.858	19.721
	SCN	20.568	24.865	26.595	27.526
	SEB-R	11.196	16.499	18.445	19.698
	SEB-N	6.122	8.263	9.526	10.117
	PEB-R	10.872	11.974	13.355	15.974
	PEB-N	10.881	11.972	13.358	15.990
	STC	24.500	25.378	23.417	22.872
	RFF	25.865	25.415	25.597	25.555
	NEB-R	17.233	17.121	16.549	17.552
	NEB-N	27.344	29.778	31.093	30.994
	PEAR **(ours)**	2.306±0.059	5.095±0.119	7.513±0.251	9.192±0.150

Table 16 Full experimental results on *sx-MA*

metric	method	layer-2	layer-3	layer-4	layer-5
KSCN	PRD	0.264	0.463	0.576	0.643
	SCN	0.570	0.697	0.721	0.738
	SEB-R	0.175	0.340	0.436	0.497
	SEB-N	0.142	0.210	0.251	0.280
	PEB-R	0.335	0.266	0.303	0.337
	PEB-N	0.334	0.266	0.303	0.337
	STC	0.733	0.703	0.696	0.696
	RFF	0.511	0.549	0.578	0.604
	NEB-R	0.458	0.431	0.403	0.371
	NEB-N	0.733	0.759	0.752	0.752
	PEAR **(ours)**	0.075±0.000	0.069±0.001	0.070±0.002	0.073±0.001
KSND	PRD	0.019	0.039	0.074	0.103
	SCN	0.551	0.575	0.558	0.542
	SEB-R	0.018	0.047	0.084	0.119
	SEB-N	0.018	0.051	0.081	0.108
	PEB-R	0.028	0.067	0.103	0.144
	PEB-N	0.028	0.067	0.103	0.144
	STC	0.517	0.494	0.475	0.481
	RFF	0.407	0.424	0.419	0.414
	NEB-R	0.158	0.157	0.165	0.170
	NEB-N	0.240	0.268	0.236	0.244
	PEAR **(ours)**	0.149±0.001	0.169±0.001	0.153±0.001	0.114±0.001
DACC	PRD	0.113	0.135	0.146	0.162
	SCN	0.434	0.514	0.580	0.564
	SEB-R	0.090	0.113	0.125	0.143
	SEB-N	0.082	0.097	0.108	0.122
	PEB-R	0.134	0.051	0.027	0.042
	PEB-N	0.133	0.051	0.027	0.042
	STC	0.173	0.141	0.134	0.143
	RFF	0.442	0.475	0.482	0.472
	NEB-R	0.129	0.106	0.090	0.087
	NEB-N	0.191	0.169	0.162	0.171
	PEAR **(ours)**	0.071±0.002	0.062±0.002	0.034±0.001	0.004±0.004
NetSimile	PRD	7.317	11.563	14.668	16.403
	SCN	20.317	22.851	23.891	24.019
	SEB-R	6.035	11.508	14.621	16.059
	SEB-N	5.275	8.677	10.356	11.333
	PEB-R	9.545	10.886	14.598	16.204
	PEB-N	9.531	10.886	14.597	16.201
	STC	24.303	25.971	26.068	25.792
	RFF	20.941	20.592	20.722	21.213
	NEB-R	15.878	15.291	13.433	12.214
	NEB-N	24.828	28.615	27.732	27.321
	PEAR **(ours)**	7.596±0.066	9.347±0.080	9.908±0.022	10.736±0.021

Table 17 Full experimental results on *sx-SO*

metric	method	layer-2	layer-3	layer-4	layer-5
KSCN	PRD	0.153	0.264	0.303	0.315
	SCN	0.682	0.812	0.841	0.845
	SEB-R	0.230	0.338	0.329	0.322
	SEB-N	0.103	0.154	0.179	0.200
	PEB-R	0.202	0.067	0.146	0.131
	PEB-N	0.202	0.067	0.146	0.131
	STC	0.481	0.385	0.336	0.317
	RFF	0.690	0.736	0.753	0.757
	NEB-R	0.402	0.295	0.266	0.254
	NEB-N	0.081	0.117	0.166	0.185
	PEAR **(ours)**	0.191±0.000	0.275±0.003	0.258±0.002	0.231±0.001
KSND	PRD	0.015	0.025	0.031	0.037
	SCN	0.267	0.359	0.412	0.446
	SEB-R	0.013	0.027	0.047	0.064
	SEB-N	0.020	0.034	0.040	0.043
	PEB-R	0.033	0.081	0.083	0.086
	PEB-N	0.033	0.081	0.083	0.086
	STC	0.626	0.553	0.496	0.451
	RFF	0.160	0.226	0.277	0.320
	NEB-R	0.376	0.373	0.335	0.299
	NEB-N	0.338	0.218	0.160	0.115
	PEAR **(ours)**	0.070±0.000	0.150±0.003	0.227±0.005	0.264±0.004
DACC	PRD	0.036	0.037	0.036	0.036
	SCN	0.394	0.507	0.572	0.607
	SEB-R	0.037	0.037	0.035	0.035
	SEB-N	0.026	0.026	0.026	0.027
	PEB-R	0.040	0.004	0.029	0.022
	PEB-N	0.040	0.004	0.029	0.022
	STC	0.049	0.035	0.030	0.029
	RFF	0.535	0.549	0.554	0.555
	NEB-R	0.036	0.021	0.020	0.020
	NEB-N	0.007	0.034	0.040	0.041
	PEAR **(ours)**	0.037±0.000	0.039±0.000	0.036±0.000	0.035±0.000

Table 18 Full experimental results on *sx-SU*

metric	method	layer-2	layer-3	layer-4	layer-5
KSCN	PRD	0.209	0.305	0.332	0.350
	SCN	0.683	0.787	0.804	0.797
	SEB-R	0.279	0.343	0.338	0.350
	SEB-N	0.170	0.228	0.259	0.290
	PEB-R	0.245	0.099	0.118	0.156
	PEB-N	0.245	0.099	0.118	0.156
	STC	0.416	0.352	0.331	0.350
	RFF	0.698	0.721	0.721	0.713
	NEB-R	0.416	0.355	0.338	0.346
	NEB-N	0.426	0.265	0.203	0.215
	PEAR **(ours)**	0.020±0.001	0.079±0.003	0.135±0.003	0.178±0.001
KSND	PRD	0.029	0.045	0.049	0.059
	SCN	0.380	0.491	0.561	0.594
	SEB-R	0.024	0.052	0.066	0.084
	SEB-N	0.029	0.040	0.042	0.052
	PEB-R	0.043	0.069	0.062	0.056
	PEB-N	0.043	0.069	0.062	0.056
	STC	0.450	0.368	0.312	0.287
	RFF	0.339	0.401	0.440	0.461
	NEB-R	0.241	0.203	0.171	0.162
	NEB-N	0.286	0.202	0.094	0.079
	PEAR **(ours)**	0.038±0.000	0.022±0.002	0.006±0.000	0.020±0.002
DACC	PRD	0.047	0.047	0.046	0.048
	SCN	0.462	0.587	0.637	0.670
	SEB-R	0.051	0.048	0.045	0.047
	SEB-N	0.038	0.038	0.039	0.041
	PEB-R	0.053	0.006	0.008	0.003
	PEB-N	0.052	0.006	0.008	0.003
	STC	0.058	0.042	0.039	0.046
	RFF	0.580	0.597	0.602	0.601
	NEB-R	0.061	0.046	0.043	0.044
	NEB-N	0.064	0.014	0.023	0.022
	PEAR **(ours)**	0.007±0.001	0.019±0.001	0.029±0.001	0.036±0.000

Table 18 (continued)

metric	method	layer-2	layer-3	layer-4	layer-5
NetSimile	PRD	9.091	14.961	18.101	19.421
	SCN	22.053	25.600	26.827	27.314
	SEB-R	11.720	17.238	19.592	20.977
	SEB-N	8.601	12.653	14.380	15.773
	PEB-R	11.031	12.729	14.306	16.530
	PEB-N	11.019	12.727	14.306	16.530
	STC	25.350	25.761	24.815	24.382
	RFF	24.993	25.270	25.487	25.930
	NEB-R	19.497	19.244	19.118	19.210
	NEB-N	24.957	20.922	22.447	21.625
	PEAR **(ours)**	2.588±0.318	4.736±0.104	7.787±0.184	10.352±0.053

Table 19 Full experimental results on *co-DB*

metric	method	layer-2	layer-3	layer-4	layer-5
KSCN	PRD	0.577	0.697	0.693	0.658
	SCN	0.586	0.677	0.693	0.690
	SEB-R	0.484	0.494	0.491	0.469
	SEB-N	0.249	0.172	0.122	0.079
	PEB-R	0.609	0.537	0.504	0.465
	PEB-N	0.609	0.537	0.504	0.465
	STC	0.065	0.143	0.330	0.413
	RFF	0.431	0.310	0.245	0.188
	NEB-R	0.091	0.037	0.103	0.152
	NEB-N	0.144	0.207	0.253	0.293
	PEAR **(ours)**	0.046±0.000	0.206±0.015	0.439±0.027	0.626±0.010
KSND	PRD	0.183	0.226	0.259	0.279
	SCN	0.356	0.336	0.296	0.256
	SEB-R	0.177	0.228	0.255	0.264
	SEB-N	0.118	0.158	0.171	0.171
	PEB-R	0.213	0.285	0.304	0.295
	PEB-N	0.213	0.285	0.304	0.295
	STC	0.230	0.247	0.339	0.410
	RFF	0.328	0.227	0.177	0.135
	NEB-R	0.109	0.050	0.029	0.032
	NEB-N	0.158	0.067	0.048	0.086
	PEAR **(ours)**	0.064±0.000	0.024±0.006	0.078±0.013	0.255±0.019

Table 19 (continued)

metric	method	layer-2	layer-3	layer-4	layer-5
DACC	PRD	0.398	0.392	0.361	0.329
	SCN	0.152	0.159	0.165	0.164
	SEB-R	0.309	0.286	0.257	0.231
	SEB-N	0.126	0.062	0.022	0.007
	PEB-R	0.419	0.361	0.315	0.279
	PEB-N	0.419	0.361	0.315	0.279
	STC	0.057	0.083	0.135	0.192
	RFF	0.287	0.212	0.163	0.126
	NEB-R	0.043	0.018	0.055	0.087
	NEB-N	0.106	0.037	0.086	0.120
	PEAR **(ours)**	0.087±0.000	0.206±0.009	0.294±0.008	0.322±0.002
NetSimile	PRD	16.247	19.705	21.321	22.057
	SCN	10.478	12.207	13.520	14.262
	SEB-R	15.753	18.051	18.579	18.591
	SEB-N	13.166	15.778	17.544	17.731
	PEB-R	17.155	17.291	19.982	19.609
	PEB-N	17.074	17.287	19.966	19.612
	STC	19.979	19.511	22.531	23.371
	RFF	20.067	15.482	12.799	10.487
	NEB-R	11.914	9.378	8.875	8.742
	NEB-N	21.978	19.250	18.583	18.255
	PEAR **(ours)**	9.209±0.009	14.024±0.066	16.830±0.191	22.859±0.727

Table 20 Full experimental results on *co-GE*

metric	method	layer-2	layer-3	layer-4	layer-5
KSCN	PRD	0.683	0.767	0.752	0.722
	SCN	0.620	0.618	0.563	0.491
	SEB-R	0.553	0.518	0.463	0.419
	SEB-N	0.299	0.221	0.160	0.117
	PEB-R	0.700	0.569	0.534	0.503
	PEB-N	0.701	0.570	0.534	0.503
	STC	0.090	0.459	0.525	0.604
	RFF	0.263	0.126	0.063	0.072
	NEB-R	0.154	0.064	0.048	0.075
	NEB-N	0.460	0.371	0.381	0.319
	PEAR **(ours)**	0.066±0.000	0.022±0.001	0.193±0.013	0.441±0.019
KSND	PRD	0.228	0.283	0.312	0.345
	SCN	0.412	0.304	0.229	0.186
	SEB-R	0.210	0.292	0.318	0.334
	SEB-N	0.171	0.210	0.207	0.202
	PEB-R	0.248	0.291	0.312	0.323
	PEB-N	0.249	0.291	0.312	0.323
	STC	0.203	0.320	0.455	0.519
	RFF	0.254	0.116	0.071	0.043
	NEB-R	0.178	0.122	0.087	0.063
	NEB-N	0.364	0.289	0.255	0.227
	PEAR **(ours)**	0.139±0.000	0.128±0.004	0.069±0.006	0.084±0.009
DACC	PRD	0.426	0.393	0.354	0.330
	SCN	0.136	0.143	0.132	0.104
	SEB-R	0.284	0.231	0.185	0.154
	SEB-N	0.083	0.009	0.034	0.059
	PEB-R	0.437	0.352	0.301	0.273
	PEB-N	0.437	0.353	0.301	0.273
	STC	0.125	0.215	0.215	0.267
	RFF	0.220	0.129	0.080	0.052
	NEB-R	0.047	0.008	0.037	0.055
	NEB-N	0.267	0.177	0.148	0.107
	PEAR **(ours)**	0.028±0.000	0.049±0.007	0.164±0.006	0.266±0.005

Table 20 (continued)

metric	method	layer-2	layer-3	layer-4	layer-5
NetSimile	PRD	16.932	19.968	20.996	21.830
	SCN	12.804	13.911	13.827	12.727
	SEB-R	16.439	18.021	17.994	18.118
	SEB-N	14.461	17.265	18.726	18.900
	PEB-R	17.500	15.756	17.848	19.084
	PEB-N	17.489	15.769	17.847	19.087
	STC	18.699	22.334	23.720	24.342
	RFF	14.022	7.388	4.724	4.033
	NEB-R	11.076	8.974	7.700	7.819
	NEB-N	24.453	22.391	20.545	19.760
	PEAR **(ours)**	8.578±0.010	8.976±0.040	12.192±0.033	13.739±0.129

Table 21 Full experimental results on *OF*

metric	method	layer-2	layer-3	layer-4	layer-5
KSCN	PRD	0.368	0.524	0.612	0.665
	SCN	0.391	0.505	0.527	0.518
	SEB-R	0.194	0.240	0.227	0.209
	SEB-N	0.336	0.472	0.533	0.560
	PEB-R	0.663	0.592	0.624	0.625
	PEB-N	0.664	0.592	0.624	0.625
	STC	0.764	0.728	0.660	0.566
	RFF	0.060	0.226	0.340	0.433
	NEB-R	0.223	0.157	0.119	0.091
	NEB-N	0.153	0.031	0.143	0.233
	PEAR **(ours)**	0.047±0.000	0.051±0.008	0.082±0.010	0.115±0.011
KSND	PRD	0.079	0.102	0.095	0.106
	SCN	0.350	0.361	0.362	0.364
	SEB-R	0.065	0.102	0.093	0.088
	SEB-N	0.069	0.096	0.102	0.116
	PEB-R	0.181	0.210	0.262	0.273
	PEB-N	0.182	0.209	0.262	0.273
	STC	0.563	0.609	0.589	0.547
	RFF	0.061	0.084	0.129	0.186
	NEB-R	0.223	0.171	0.115	0.083
	NEB-N	0.114	0.054	0.061	0.109
	PEAR **(ours)**	0.055±0.004	0.033±0.003	0.066±0.002	0.123±0.005

Table 21 (continued)

metric	method	layer-2	layer-3	layer-4	layer-5
DACC	PRD	0.183	0.271	0.334	0.377
	SCN	0.105	0.167	0.180	0.210
	SEB-R	0.044	0.062	0.069	0.067
	SEB-N	0.169	0.237	0.275	0.304
	PEB-R	0.312	0.241	0.214	0.193
	PEB-N	0.312	0.242	0.213	0.194
	STC	0.091	0.012	0.003	0.003
	RFF	0.162	0.189	0.196	0.200
	NEB-R	0.138	0.125	0.120	0.119
	NEB-N	0.053	0.028	0.019	0.013
	PEAR **(ours)**	0.059±0.004	0.125±0.008	0.200±0.008	0.247±0.015
NetSimile	PRD	7.961	12.254	13.001	14.730
	SCN	15.064	14.635	15.677	16.512
	SEB-R	6.603	9.133	10.673	10.967
	SEB-N	7.350	11.064	11.752	12.514
	PEB-R	12.233	12.537	11.849	11.488
	PEB-N	12.195	12.539	11.848	11.501
	STC	24.076	23.639	23.488	23.080
	RFF	10.795	11.329	12.851	14.079
	NEB-R	12.730	11.113	10.429	10.134
	NEB-N	7.748	4.483	4.877	7.718
	PEAR **(ours)**	5.686±0.398	6.888±0.285	8.494±0.481	11.280±0.277

Table 22 Full experimental results on *FL*

metric	method	layer-2	layer-3	layer-4	layer-5
KSCN	PRD	0.438	0.581	0.592	0.476
	SCN	0.600	0.704	0.656	0.686
	SEB-R	0.355	0.411	0.452	0.386
	SEB-N	0.208	0.208	0.206	0.114
	PEB-R	0.485	0.404	0.323	0.260
	PEB-N	0.485	0.404	0.323	0.260
	STC	0.545	0.474	0.445	0.433
	RFF	0.335	0.283	0.147	0.178
	NEB-R	0.361	0.345	0.373	0.278
	NEB-N	0.428	0.485	0.603	N/A
	PEAR **(ours)**	0.064±0.007	0.166±0.019	0.261±0.033	0.474±0.021
KSND	PRD	0.058	0.131	0.185	0.283
	SCN	0.527	0.438	0.437	0.293
	SEB-R	0.069	0.166	0.208	0.277
	SEB-N	0.062	0.133	0.144	0.146
	PEB-R	0.077	0.145	0.197	0.269
	PEB-N	0.077	0.145	0.197	0.269
	STC	0.302	0.408	0.378	0.451
	RFF	0.245	0.166	0.089	0.084
	NEB-R	0.104	0.118	0.119	0.092
	NEB-N	0.149	0.318	0.330	N/A
	PEAR **(ours)**	0.056±0.009	0.077±0.003	0.047±0.003	0.101±0.006
DACC	PRD	0.229	0.197	0.180	0.130
	SCN	0.374	0.464	0.463	0.365
	SEB-R	0.174	0.123	0.136	0.106
	SEB-N	0.050	0.027	0.025	0.040
	PEB-R	0.251	0.138	0.075	0.058
	PEB-N	0.252	0.138	0.075	0.058
	STC	0.083	0.017	0.101	0.109
	RFF	0.175	0.033	0.082	0.135
	NEB-R	0.169	0.138	0.152	0.110
	NEB-N	0.091	0.077	0.187	N/A
	PEAR **(ours)**	0.152±0.004	0.096±0.006	0.063±0.014	0.011±0.005
NetSimile	PRD	11.776	16.235	18.447	20.785
	SCN	20.167	21.877	20.421	19.757
	SEB-R	12.433	15.503	17.805	19.317
	SEB-N	10.020	12.392	14.086	12.641
	PEB-R	13.722	13.137	15.493	14.071
	PEB-N	13.760	13.141	15.493	14.071
	STC	20.606	21.186	19.798	23.037
	RFF	14.230	16.560	14.197	10.233
	NEB-R	13.182	12.921	13.251	12.441
	NEB-N	15.381	19.241	22.776	N/A
	PEAR **(ours)**	7.688±0.368	8.318±0.302	8.965±0.462	10.700±1.054

Supplementary information The online version contains supplementary material available at (https://doi.org/10.1007/s10618-023-00940-w).

Funding This work was supported by National Research Foundation of Korea (NRF) grant funded by the Korea government (MSIT) (No. NRF-2020R1C1C1008296) and Institute of Information & Communications Technology Planning & Evaluation (IITP) grant funded by the Korea government (MSIT) (No. 2022-0-00871, Development of AI Autonomy and Knowledge Enhancement for AI Agent Collaboration) (No. 2019-0-00075, Artificial Intelligence Graduate School Program (KAIST)).

Declarations

Conflict of interest The authors have no relevant financial or non-financial interests to disclose.

References

Adamic LA, Adar E (2003) Friends and neighbors on the web. Soc Netw 25(3):211–230
Adriaens F, De Bie T, Gionis A et al (2020) Relaxing the strong triadic closure problem for edge strength inference. Data Min Knowl Disc 34(3):611–651
Ahmad I, Akhtar MU, Noor S et al (2020) Missing link prediction using common neighbor and centrality based parameterized algorithm. Sci Rep 10(1):1–9
Aicher C, Jacobs AZ, Clauset A (2015) Learning latent block structure in weighted networks. J Comp Netw 3(2):221–248
Aittokallio T, Schwikowski B (2006) Graph-based methods for analysing networks in cell biology. Brief Bioinform 7(3):243–255
Akoglu L, Tong H, Koutra D (2015) Graph based anomaly detection and description: a survey. Data Min Knowl Disc 29(3):626–688
Akoglu L, McGlohon M, Faloutsos C (2008) Rtm: Laws and a recursive generator for weighted time-evolving graphs. In: ICDM
Albert R, Barabási AL (2002) Statistical mechanics of complex networks. Rev Mod Phys 74(1):47
Barrat A, Barthélemy M, Vespignani A (2004) Modeling the evolution of weighted networks. Phys. Rev. E 70(6):066149
Benson AR, Gleich DF, Leskovec J (2016) Higher-order organization of complex networks. Science 353(6295):163–166
Benson AR, Abebe R, Schaub MT et al (2018) Simplicial closure and higher-order link prediction. PNAS 115(48):E11221–E11230
Berlingerio M, Koutra D, Eliassi-Rad T, et al (2012) Netsimile: A scalable approach to size-independent network similarity. arXiv:1209.2684
Berry JW, Hendrickson B, LaViolette RA et al (2011) Tolerating the community detection resolution limit with edge weighting. Phys. Rev. E 83(5):056119
Blondel VD, Guillaume JL, Lambiotte R et al (2008) Fast unfolding of communities in large networks. J Stat Mech Theor Experiment 10:P10008
Bonacich P (1987) Power and centrality: a family of measures. Am J Sociol 92(5):1170–1182
Breiman L (2001) Random forests. Mach Learn 45(1):5–32
Bu F, Kang S, Shin K (2022) Code, datasets, and online appendix. https://github.com/bokveizen/topology-edge-weight-interplay
Cao S, Lu W, Xu Q (2015) Grarep: Learning graph representations with global structural information. In: CIKM
Chakrabarti D, Faloutsos C (2006) Graph mining: laws, generators, and algorithms. ACM Comput Surv (CSUR). https://doi.org/10.1145/1132952.1132954
Cleaver F (2002) Reinventing institutions: bricolage and the social embeddedness of natural resource management. Eur J Develop Res 14(2):11–30
De Montis A, Barthélemy M, Chessa A et al (2007) The structure of interurban traffic: a weighted network analysis. Environ Plann B Plann Des 34(5):905–924
Fey M, Lenssen JE (2019) Fast graph representation learning with pytorch geometric. arXiv preprint arXiv:1903.02428

Fire M, Tenenboim L, Lesser O, et al (2011) Link prediction in social networks using computationally efficient topological features. In: PASSAT/SocialCom
Fortunato S (2010) Community detection in graphs. Phys Rep 486(3–5):75–174
Freeman LC (1977) A set of measures of centrality based on betweenness. Sociometry 40(1):35–41
Fu C, Zhao M, Fan L et al (2018) Link weight prediction using supervised learning methods and its application to yelp layered network. TKDE 30(8):1507–1518
Garner WR, McGill WJ (1956) The relation between information and variance analyses. Psychometrika 21(3):219–228
Girvan M, Newman ME (2002) Community structure in social and biological networks. PNAS 99(12):7821–7826
Grover A, Leskovec J (2016) node2vec: Scalable feature learning for networks. In: KDD
Gunes I, Gunduz-Oguducu S, Cataltepe Z (2016) Link prediction using time series of neighborhood-based node similarity scores. Data Min Knowl Discov 30:147–180
Harary F, Norman RZ (1960) Some properties of line digraphs. Rendiconti del circolo matematico di palermo 9(2):161–168
He Z, Chen W, Wei X et al (2021) On the statistical significance of communities from weighted graphs. Sci Rep 11(1):20304
Heath LS, Parikh N (2011) Generating random graphs with tunable clustering coefficients. Physica A 390(23–24):4577–4587
Jeh G, Widom J (2003) Scaling personalized web search. In: TheWebConf (WWW)
Kılıç B, Özturan C, Şen A (2022) Parallel analysis of ethereum blockchain transaction data using cluster computing. Clust Comput 25(3):1885–1898
Kılıç B, Özturan C, Şen A (2022a) Analyzing large-scale blockchain transaction graphs for fraudulent activities. In: Big Data and Artificial Intelligence in Digital Finance. Springer, p 253–267
Kumar R, Liu P, Charikar M, et al (2020) Retrieving top weighted triangles in graphs. In: WSDM
Kumar S, Spezzano F, Subrahmanian V, et al (2016) Edge weight prediction in weighted signed networks. In: ICDM
Leicht EA, Holme P, Newman ME (2006) Vertex similarity in networks. Phys Rev E 73(2):026120
Leskovec J, Chakrabarti D, Kleinberg J, et al (2005) Realistic, mathematically tractable graph generation and evolution, using kronecker multiplication. In: ECML PKDD
Levandowsky M, Winter D (1971) Distance between sets. Nature 234(5323):34–35
Liu Z, Zhang QM, Lü L et al (2011) Link prediction in complex networks: a local naïve bayes model. EPL 96(4):48007
Liu R, Feng S, Shi R et al (2014) Weighted graph clustering for community detection of large social networks. Procedia Comput Sci 31:85–94
Liu J, Shang M, Chen D (2009) Personal recommendation based on weighted bipartite networks. In: FSKD
Martínez V, Berzal F, Cubero JC (2016) A survey of link prediction in complex networks. CSUR 49(4):1–33
McGlohon M, Akoglu L, Faloutsos C (2008) Weighted graphs and disconnected components: patterns and a generator. In: KDD
Newman ME (2004) Analysis of weighted networks. Phys Rev E 70(5):056131
Opsahl T (2011) Why anchorage is not (that) important: Binary ties and sample selection. https://toreopsahl.com/2011/08/12/why-anchorage-is-not-that-important-binary-ties-and-sample-selection/
Opsahl T (2013) Triadic closure in two-mode networks: redefining the global and local clustering coefficients. Soc Netw 35(2):159–167
Page L, Brin S, Motwani R et al (1999) The pagerank citation ranking: Bringing order to the web. Stanford InfoLab, California
Paranjape A, Benson AR, Leskovec J (2017) Motifs in temporal networks. In: WSDM
Pei H, Wei B, Chang KCC, et al (2020) Geom-gcn: Geometric graph convolutional networks. In: ICLR
Ravasz E, Somera AL, Mongru DA et al (2002) Hierarchical organization of modularity in metabolic networks. Science 297(5586):1551–1555
Rotabi R, Kamath K, Kleinberg J, et al (2017) Detecting strong ties using network motifs. In: Proceedings of the 26th international conference on world wide web companion
Rozemberczki B, Kiss O, Sarkar R (2020) Karate Club: An API Oriented Open-source Python Framework for Unsupervised Learning on Graphs. In: CIKM
Salton G, McGill MJ (1983) Introduction to modern information retrieval. McGraw-Hill, New York
Sanei-Mehri SV, Sariyuce AE, Tirthapura S (2018) Butterfly counting in bipartite networks. In: KDD

Satuluri V, Parthasarathy S, Ruan Y (2011) Local graph sparsification for scalable clustering. SIGMOD
Seidman SB (1983) Network structure and minimum degree. Soc Netw 5(3):269–287
Sen P, Namata G, Bilgic M et al (2008) Collective classification in network data. AI Mag 29(3):93–93
Shchur O, Mumme M, Bojchevski A, et al (2018) Pitfalls of graph neural network evaluation. arXiv preprint arXiv:1811.05868
Shin K, Oh S, Kim J et al (2020) Fast, accurate and provable triangle counting in fully dynamic graph streams. TKDD 14(2):1–39
Shuai HH, Yang DN, Philip SY, et al (2013) On pattern preserving graph generation. In: ICDM
Sinha A, Shen Z, Song Y, et al (2015) An overview of microsoft academic service (mas) and applications. In: TheWebConf (WWW)
Sintos S, Tsaparas P (2014) Using strong triadic closure to characterize ties in social networks. In: KDD
Skarkala ME, Maragoudakis M, Gritzalis S, et al (2012) Privacy preservation by k-anonymization of weighted social networks. In: ASONAM
Sorensen TA (1948) A method of establishing groups of equal amplitude in plant sociology based on similarity of species content and its application to analyses of the vegetation on danish commons. Biologiske Skrifter 5(4):1–34
Starnini M, Lepri B, Baronchelli A, et al (2017) Robust modeling of human contact networks across different scales and proximity-sensing techniques. In: SocInfo 2017
Steinhaeuser K, Chawla NV (2008) Community detection in a large real-world social network. In: Social computing, behavioral modeling, and prediction
Tate RF (1954) Correlation between a discrete and a continuous variable point-biserial correlation. Ann Math Stat 25(3):603–607
Thottan M, Liu G, Ji C (2010) Anomaly detection approaches for communication networks. In: Algorithms for next generation networks
Tsourakakis CE (2008) Fast counting of triangles in large real networks without counting: Algorithms and laws. In: ICDM
Tsourakakis CE, Pachocki J, Mitzenmacher M (2017) Scalable motif-aware graph clustering. In: TheWebConf (WWW)
Wang P, Xu B, Wu Y et al (2015) Link prediction in social networks: the state-of-the-art. Sci China Inf Sci 58(1):1–38
Watts DJ, Strogatz SH (1998) Collective dynamics of small-world networks. Nature 393(6684):440–442
Wills P, Meyer FG (2020) Metrics for graph comparison: a practitioner's guide. Plos one 15(2):e0228728
Yang R, Sala F, Bogdan P (2021) Hidden network generating rules from partially observed complex networks. Commun Phys 4(1):1–12
Zhang Z, Cui P, Li H, et al (2018) Billion-scale network embedding with iterative random projection. In: ICDM
Zhao J, Miao L, Yang J et al (2015) Prediction of links and weights in networks by reliable routes. Sci Rep 5(1):1–15
Zhou T, Lü L, Zhang YC (2009) Predicting missing links via local information. Eur Phys J B 71(4):623–630
Zhu B, Xia Y (2016) Link prediction in weighted networks: a weighted mutual information model. PloS one 11(2):e0148265
Zhu B, Xia Y, Zhang XJ (2016) Weight prediction in complex networks based on neighbor set. Sci Rep 6(1):1–10